DOI:10.14753/SE.2017.2079

The role of novel iterative image reconstruction algorithms in coronary CT imaging

Doctoral Thesis

Bálint Szilveszter M.D.

Semmelweis University
Doctoral School of Basic Medicine

Supervisor: Pál Maurovich-Horvat, M.D., Ph.D.

Official reviewers: Tamás Györke, M.D., Ph.D.
Gergely Ágoston, M.D., Ph.D.

Head of the Final Examination Committee:
Viktor Bérczi, M.D., D.Sc.

Members of the Final Examination Committee:
Attila Doros, M.D., Ph.D.
László Sallai, M.D., Ph.D.

Budapest
2017

DOI:10.14753/SE.2017.2079

Table of Contents

DOI:10.14753/SE.2017.2079

DOI:10.14753/SE.2017.2079

Abbreviations

ACS	Acute Coronary Syndrome
AHA	American Heart Association
ALARA	As Low As Reasonably Achievable
BMI	Body Mass Index
bpm	beat per minute
CAC	Coronary Artery Calcium
CAD	Coronary Artery Disease
CI	Confidence Interval
CNR	Contrast-to-noise ratio
CT	Computed Tomography
CTA	Computed Tomography Angiography
CVD	Cardiovascular Disease
ECG	Electrocardiography
FBP	Filtered Back Projection
HIR	Hybrid-type Iterative Reconstruction
HR	Heart Rate
HU	Hounsfield Unit
ICA	Invasive Coronary Angiography
ICC	Intraclass Correlation Coefficient
IMR	Iterative Model Reconstruction
IR	Iterative Reconstruction
IRB	Institutional Review Board
kV	kilovolt
LAD	Left Anterior Descending Artery
LCX	Left Circumflex Artery
LM	Left Main Coronary Artery
mAs	milliampere-second
mm Hg	millimeter of mercury
MPR	Multiplanar Reformation
NCP	Non-calcified Plaque
NRS	Napkin-ring sign

DOI:10.14753/SE.2017.2079

PL	Posterolateral Branch
RCA	Right Coronary Artery
ROI	Region of Interest
SCCT	Society of Cardiovascular Computed Tomography
SNR	Signal-to-noise Ratio
TCFA	Thin Cap Fibroatheroma
VH-IVUS	Virtual-Histology Intravascular Ultrasound

DOI:10.14753/SE.2017.2079

1. INTRODUCTION

Cardiovascular disease (CVD) is the leading cause of morbidity and mortality globally (1-3). CVD is responsible for over 4 million deaths in Europe, accounting for 47 % of all deaths (4). Coronary artery disease (CAD) is a dynamic process of atherosclerosis that could lead to acute or chronic luminal obstruction of the coronaries (5). Prevalence of CAD is expected to increase by 10 % in the upcoming years and health care costs are expected to escalate correspondingly (6,7). Therefore, the growing incidence and prevalence of CAD necessitate the implementation of effective prevention strategies based on noninvasive diagnostic tools in order to improve these devastating statistics and reduce the economic burden on healthcare systems. Unfortunately, the currently applied noninvasive diagnostic modalities have limited diagnostic accuracy to detect obstructive CAD (8).

In recent decades coronary computed tomography (CT) angiography (CTA) has emerged as a highly reliable and non-invasive modality for the detection of coronary artery disease. Prior landmark studies have extensively validated the diagnostic accuracy of coronary CTA versus the gold standard invasive coronary angiography (ICA). Investigations have consistently demonstrated the excellent negative predictive value of CTA (9,10). Accordingly, the main indication for coronary CTA is to rule out CAD in patients with low-to intermediate pre-test probability (9,11). Current CT scanners with high temporal and spatial resolution are able to detect significantly more coronary lesions than ICA and are also able to depict adjacent cardiac and non-cardiac structures with great certainty. Importantly, coronary CTA is currently the only non-invasive imaging modality that can describe the extent, distribution and severity of non-obstructive CAD which has significant prognostic implications for patients with stable or acute chest pain (12,13). Furthermore, CTA is a promising modality for functional evaluation of coronary lesions using cutting-edge technologies such as CT-derived fractional flow reserve simulation and dynamic CT perfusion imaging.

Due to technological advancements, coronary CTA imaging allows for robust qualitative and quantitative assessment of atherosclerotic plaques. Moreover, CTA is a potential tool to monitor morphological intraplaque changes over time using serial imaging. There are different methods to evaluate the extent and severity of CAD. Coronary artery calcium

(CAC) scores measured by CT is a widely utilized, simple, reliable and useful tool for describing coronary plaque burden and is also considered as a screening method for asymptomatic patients. Notably, recent studies suggest that CAC scoring has the ability to also re-stratify patient's risk and improve statin eligibility. Nonzero calcium score is associated with higher probability for obstructive CAD and increased risk for adverse cardiac events. Consequently, guidelines also incorporated CAC scoring to be considered if conventional risk assessment is uncertain (Class IIb recommendation in the European Society of Cardiology guidelines). CAC scores are measured using non-contrast CT images, however, subsequent contrast enhanced CTA of the coronaries also allows further differentiation of non-calcified or partially calcified plaques in the coronary system based on plaque composition. Moreover, qualitative and quantitative high-risk plaque features were introduced in clinical practice to identify prone-to-rupture coronary plaques.

The number of diagnostic cardiac tests has increased substantially in recent years and this has led to concerns attributable to increased radiation exposure. We have to ensure diagnostic image quality for all patients with lowest dose exposure reasonable achievable according to the "as low as reasonably achievable" (ALARA) principle. There are several dose saving techniques and protocols that were introduced in daily practice to minimize CTA related dose exposure. CAC scoring was established on traditional Filtered Back Projection (FBP) images which are currently considered outdated for contrast enhanced images as novel reconstruction algorithms with robust image noise reduction became available. The increasing use of various iterative reconstruction (IR) techniques by all vendors holds the potential to significantly reduce radiation exposure and simultaneously improve image quality of coronary CT scans. Hybrid-type and model based iterative reconstruction algorithms account for system geometry and noise statistics to eliminate noise from CT images. Despite the widespread use, the influence of novel IR algorithms on coronary calcium scoring, plaque composition and subsequent individual risk assessment remains unclear. The current thesis aims to ascertain the role of novel IR algorithms on CT based plaque assessment and risk prediction.

DOI:10.14753/SE.2017.2079

1.1 Noninvasive coronary imaging using CT angiography

Since the introduction of coronary CTA, there has been an enormous progress in scanner technology and potential clinical applications that led to an improved clinical utility of CTA (14,15). Coronary CTA in patients with suspected CAD also guides further patient management and decision making according to the recently introduced Coronary Artery Disease - Reporting and Data System guidelines (16).

Coronary CT protocol typically consists of a non-enhanced prospectively electrocardiogram (ECG) gated examination for calcium scoring followed by a subsequent contrast enhanced scan for the evaluation of the coronaries and cardiac structures. The non-enhanced scan ensures proper planning of the CTA including the length and position of the scan and the field of view. Calcification of the coronary arteries is a surrogate of coronary plaque burden and an important predictor of cardiovascular morbidity and mortality (17). CAC scoring has gained widespread acceptance due to its ability to re-stratify risk (18). Current software applications are able to calculate calcium scores, mass, volume or even intensity. The scoring method was described by Agatston and is calculated from the calcified lesion area weighted by a density factor based on the voxel with the highest density (19). Non-contrast images with 3 mm slice thickness are reconstructed with filtered back projection to quantify coronary calcium. Despite the fact that calcium scoring does not account for non-calcified plaques it is an excellent tool to predict future outcomes: 0-10 CAC score is considered low risk for adverse events or obstructive CAD, between 10-100 means approximately 2.5 times higher risk, between 100-400 3.5 times higher risk, between 400-1000 6 times higher risk and above 1000 12 times higher risk for cardiovascular mortality within 5 years (20,21).

In a subsequent step with the administration of iodinated contrast material robust qualitative and quantitative characterization coronary plaques is feasible (22). High resolution CT scanners are able to depict the vessel wall and the atherosclerotic plaques **(Figure 1)**. Also, functional assessment of the heart is highly reproducible using CTA images. CT angiography is widely used to describe the calcification of valves, or to provide spatial information for the electro-anatomical mapping during radiofrequency ablation procedures. In this regards, readers are also able to exclude left atrial appendage thrombus or changes in atrial structures. Importantly, coronary CTA images provide

DOI:10.14753/SE.2017.2079

additional information on extracardiac findings of adjacent organs including the lungs, diaphragm, mediastinum or the liver and spleen.

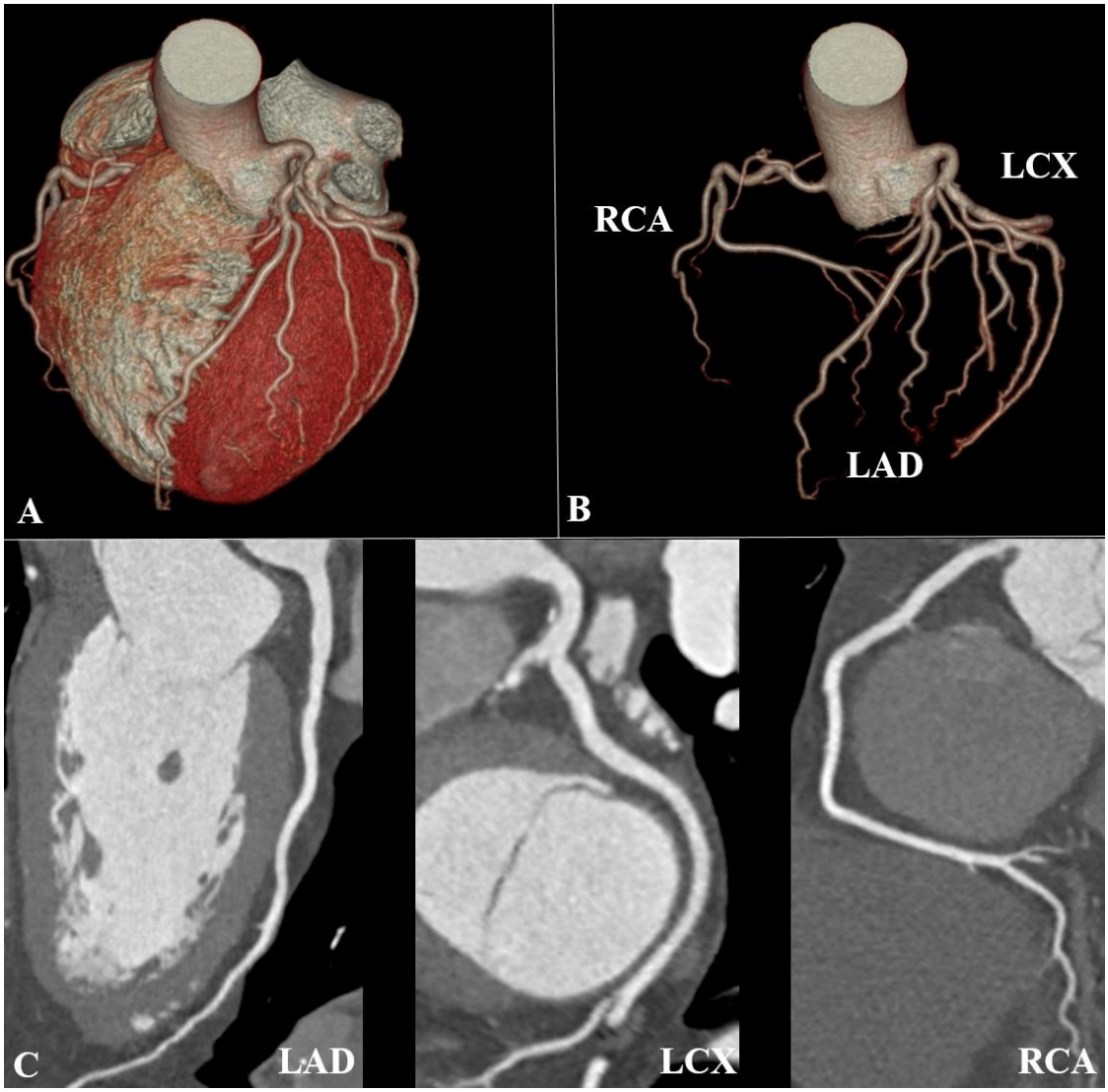

Figure 1. Curved multiplanar and 3D volume-rendered images of the coronary arteries and the heart *(own material)*

A: 3D volumetric reconstruction of the heart and coronaries B: 3D coronary tree C: Multiplanar curved reconstruction image of the 3 main epicardial coronaries

LAD: left anterior descending artery; LCX: left circumflex artery; RCA: right coronary artery

DOI:10.14753/SE.2017.2079

Guidelines for the reading and reporting of coronary findings are described in the Society of Cardiovascular Computed Tomography (SCCT) guidelines (23,24). Coronary lesions are evaluated on a segmental basis using the modified American Heart Association (AHA) 18-segment classification scheme. When analyzing CTA images, segment based assessment of the degree of luminal stenosis is crucial. The degree of stenosis can be evaluated using a 5-point scale as follows: minimal 1-24% stenosis, mild 25-49% stenosis, moderate 50-69% stenosis, severe 70-99% stenosis and occlusion 100% stenosis. Representative examples for stenosis categories are shown on **Figure 2**.

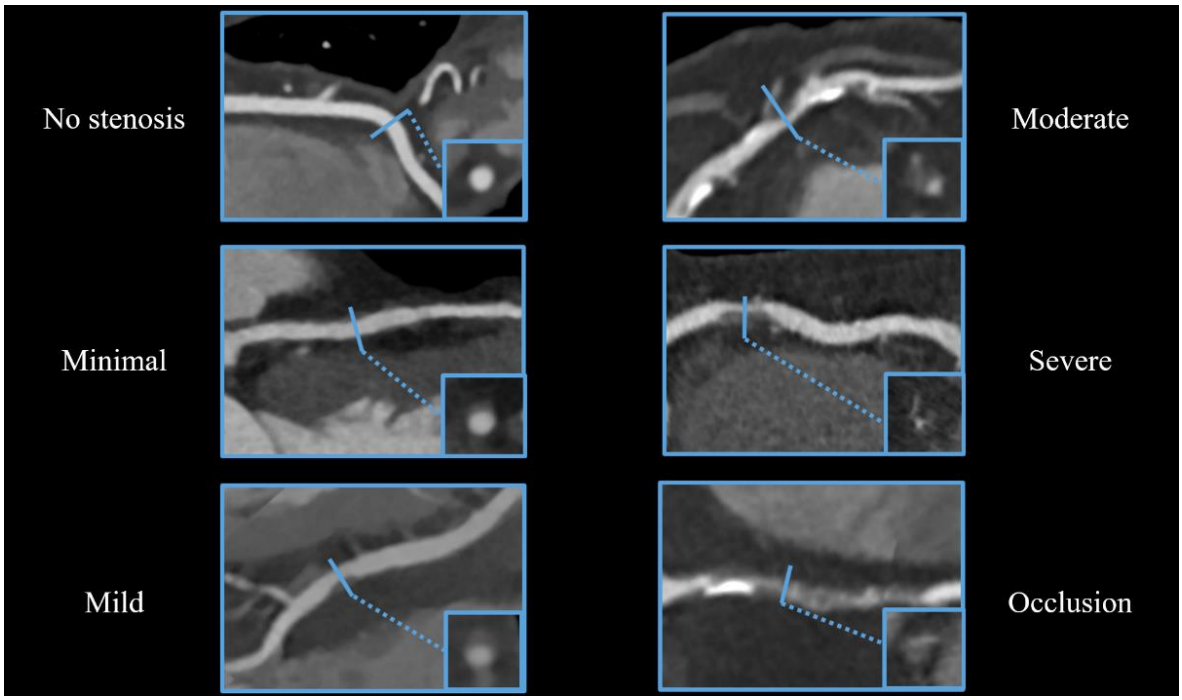

Figure 2. Representative images for stenosis classification using CTA images *(own material)*.

Based on coronary CTA images we can distinguish between no stenosis (0%), minimal 1-24% stenosis, mild 25-49% stenosis, moderate 50-69% stenosis, severe 70-99% stenosis and occlusion 100%. Cross-sectional images are depicted in the boxes for each category.

DOI:10.14753/SE.2017.2079

On qualitative plaque assessment, we can distinguish between calcified, non-calcified or partially calcified plaques based on the extent of calcification in a given plaque (**Figure 3)**. Also, current guidelines strongly encourage the assessment of high-risk plaque features such as positive remodeling, spotty calcium, napkin-ring sign (NRS) or low attenuation plaque (16). High-risk plaques seem to possess a higher risk for rupture and thus, could lead to sudden luminal thrombosis and acute myocardial infarction (25). Optimal patient management is dependent on the prognostic information provided by CTA. Comprehensive assessment of the extent, location, characteristics and severity of CAD using CTA images has prognostic relevance for patients with chest pain (13).

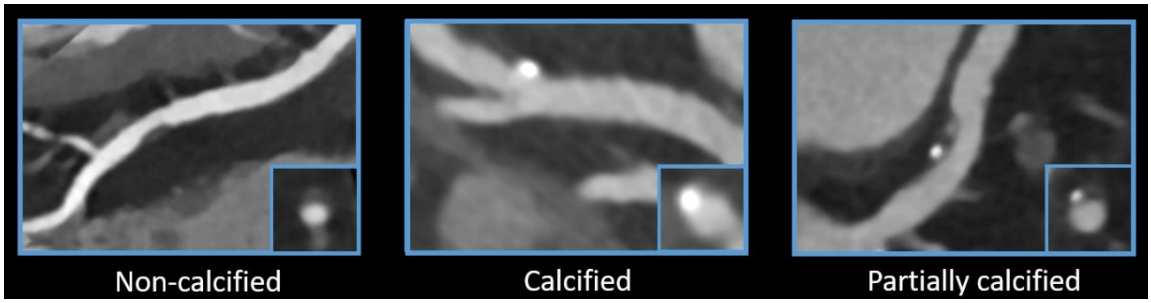

Figure 3. Qualitative plaque analysis on conventional CT reading *(own material)*.
Based on the calcium content of a given plaque we can distinguish between non-calcified, partially calcified or calcified plaques. Traditionally, coronary plaques are classified as noncalcified, partly calcified (with less than 50 % calcium) and calcified (with more than 50 % calcium) plaques on CT images.

DOI:10.14753/SE.2017.2079

1.2 Challenges of CT imaging: Radiation exposure and image quality

Radiation exposure represents a major concern in coronary CTA due to potential risk of malignancy induction (26,27). The fragile balance between diagnostic image quality and applied radiation dose is an ongoing challenge in CT imaging. Image quality is influenced by several factors including patient characteristics, scanner technology, imaging parameters (i.e. tube current, tube voltage, slice thickness) and reconstruction algorithms. Proper assessment of patient characteristics and patient preparation is therefore of utmost importance to select suitable protocol with current scanner technology (28,29). Also, frequency control with beta-blockade is necessary to reduce heart rate (HR) and heart rate variability (30). Regular and low heart rate ensures proper image quality of CTA examinations.

The multicenter Prospective Multicenter Study On Radiation Dose Estimates Of Cardiac CT Angiography in Daily Practice (PROTECTION) I study sought to evaluate the radiation dose attributed to coronary CTA ten years ago (31,32). Overall, coronary CTA was associated with a median effective dose of 12 millisievert (mSv) and investigators found a remarkable variance in applied radiation exposure levels. Accordingly, several additional milestone PROTECTION studies were carried out to evaluate the influence of dose saving strategies embedded in clinical routine and to reduce variance across CTA providers (33-35). Since then, advancements in CT scanner technology and applications have led to new opportunities of reducing dose without reducing image quality (36). CT scanners with ≥64 slice detector panels are capable to depict constantly moving coronary arteries, nowadays most centers have even more advanced scanners with dual source technology or wider detector panels to achieve excellent image quality with improved spatial resolution. Scanners are able to perform helical or axial mode synchronizing the image acquisition to the detected ECG signal (37). Retrospective ECG gating acquires images throughout the whole cardiac cycle which allows for the reconstruction of any desired cardiac phase for image analysis. Early attempts in dose savings included tube current modulation to reduce radiation exposure during retrospective gated CTA. The PROTECTION II study revealed that tube potential reduction (100 kV versus 120 kV) provides diagnostic image quality with significantly reduced exposure and thus should be

applied in non-obese patients (35). In prospective ECG triggered axial mode image acquisition is restricted to a preselected phase of the cardiac cycle typically in end-diastole, while table movement ensures total coverage of the heart in multiple steps. A comparison of retrospective and prospective ECG gated scanning mode revealed substantial reduction in radiation dose for patients with low heart rate. Later, high-pitch image acquisition mode with dual source scanners were introduced using fast table movement to cover the entire volume of the heart within one cycle. These advancements enabled submillisievert image acquisition for selected patients with low body mass index (BMI) and heart rate. In addition to scanner technology, image reconstruction techniques were improved by reintroducing the computationally intensive but powerful IR algorithms into clinical practice (38). During the past few years various iterative image reconstruction techniques have been introduced by all vendors in order to reduce radiation exposure of cardiac CT while maintaining or even improving signal to noise ratio (SNR). The impact of IR techniques on image quality and its potential to reduce radiation exposure of patients has been investigated in recent studies (39,40). Model based type of image reconstructions represents the latest advancement among image reconstruction techniques and thus limited data exists regarding the influence of this novel technique on plaque characterization and quantification. Despite recent advancements with robust noise reduction and advanced CT scanner technology, development of individualized dose saving strategies are necessary to meet the ALARA principle.

DOI:10.14753/SE.2017.2079

1.3 Coronary calcium score based risk assessment

Calcification is a common marker of atherosclerosis. CAC scoring on non-contrast CT images is an established tool for quantifying calcified atherosclerotic plaque burden. CAC assessment is therefore used for atherosclerosis screening among asymptomatic individuals with low-to-intermediate cardiovascular risk (41-44). The quantity of calcified plaques as assessed by non-contrast enhanced ECG-gated CT is an important predictor of cardiovascular morbidity and mortality. Moreover, there is a growing body of evidence that CAC scoring provides incremental value in risk prediction for adverse events of asymptomatic patients over to the conventional risk scores (45,46). Budoff et al. evaluated the prognostic utility of CAC in 25523 asymptomatic consecutive individuals (21). Long term mortality stratified by CAC score is depicted on **Figure 4** using observational data.

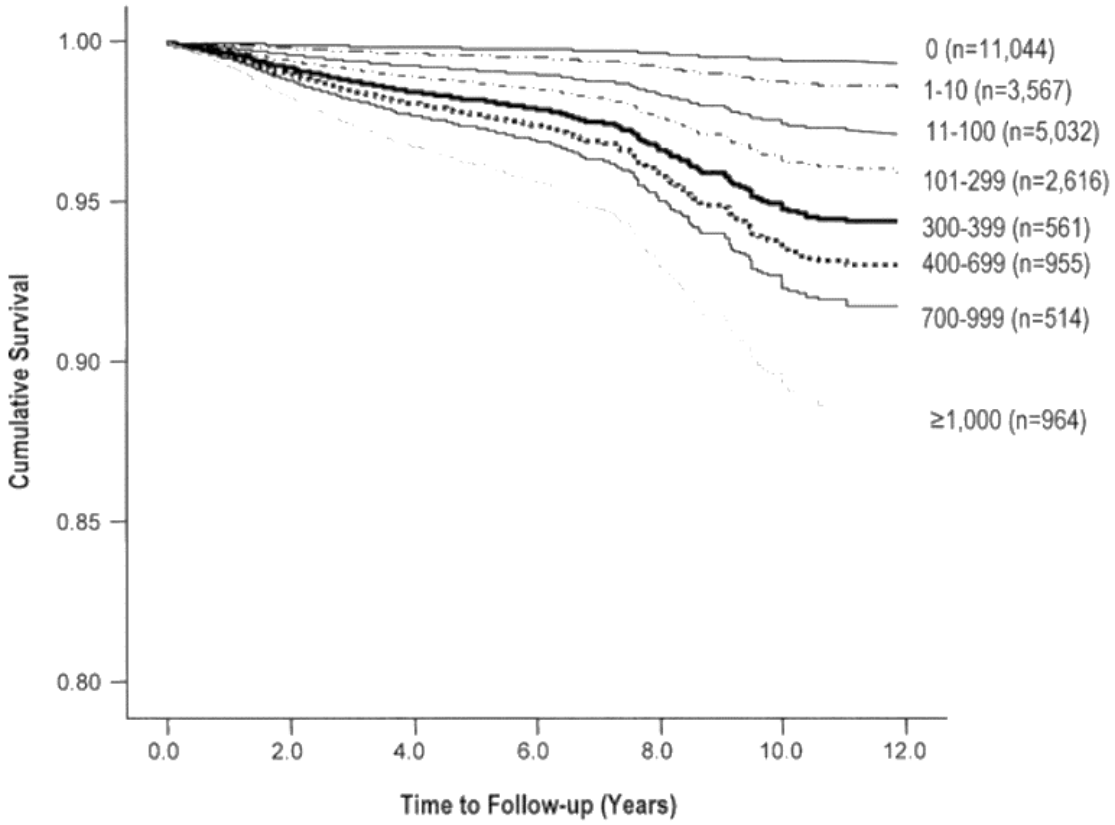

Figure 4. Prognostic value of coronary calcification by Budoff et al (21). CAC is strong independent perdictor of all cause mortality and incremental to traditional risk factors.

Zero calcium score is associated with minimal cardiovascular risk, and provides a 5 year warranty period free of major adverse cardiovascular events (47). Higher CAC scores were detected in patients with type 2 diabetes reflecting higher prevalence of CAD in this patient population. Raggi et al. demonstrated that zero calcium score in patients with diabetes is associated with similar survival rates as patients without diabetes and detectable calcium (48). CAC is also associated with non-alcoholic fatty liver disease and epicardial fat tissue volume, which has been shown to promote coronary atherosclerosis and development of high risk plaques (49-52). Furthermore, the measurement of plaque calcium density was linked to cardiovascular events in the Multi-Ethnic Study of Atherosclerosis (MESA) (53).

Notably, CAC is influenced by several factors related to image acquisition protocols (tube current, tube voltage, slice thickness), reconstruction techniques and patient characteristics (54,55). Willemink et al. demonstrated limited inter-platform reproducibility of CAC in an ex vivo study (56). CT scanners of the four major vendors measured substantially different calcium score values. Also a simulation study revealed 6.5 % risk reclassification rate among patients with intermediate cardiovascular risk. Yet, prognostic studies were based on CT images with FBP reconstruction, whereas in current clinical practice novel IR methods may underestimate cardiovascular risk estimation and have to be interpreted with caution.

DOI:10.14753/SE.2017.2079

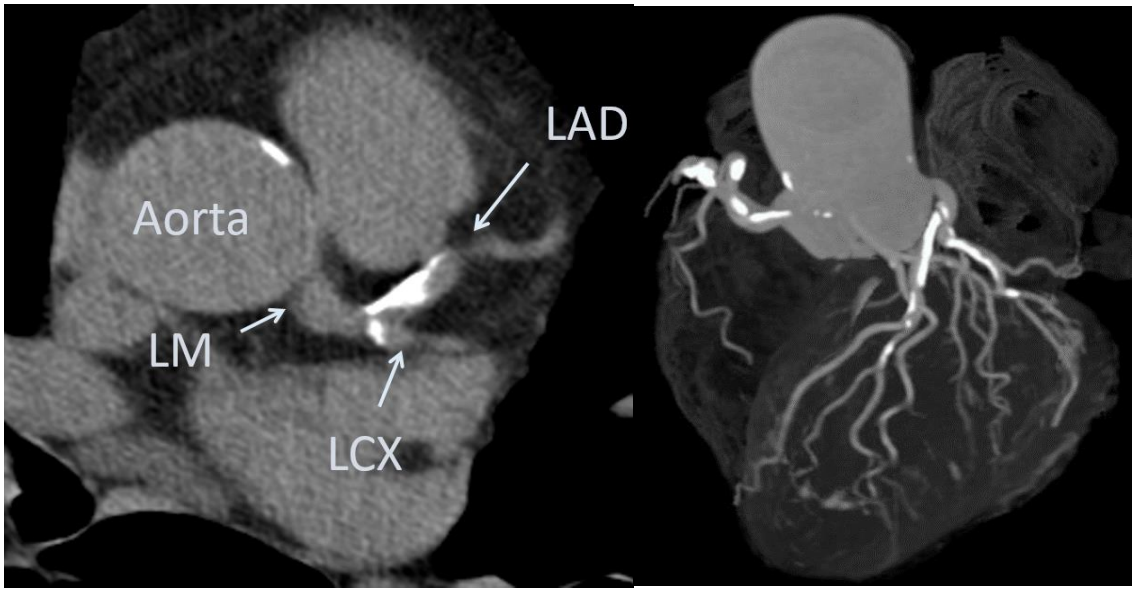

Figure 5. CAC scoring using non-contrast CT images *(own material)*.

The left panel shows a non-contrast enhanced image for calcium scoring with diffuse calcification on the left main coronary artery, left anterior descending artery and left cirxumflex artery. After manual identification of calcified plaques software provides a vessel based CAC score. On the right panel 3D volumetric reconstruction image shows the distribution of diffuse calcification along the coronary tree.

LAD: left anterior descending artery; LCX: left circumflex artery; LM: left main artery

DOI:10.14753/SE.2017.2079

1.4 Prognostic value of coronary CT angiography

In recent decades, several risk scores were proposed to estimate individual risk for CVD and adverse events (57). However, prior studies have shown that traditional risk assessment scores, such as the widely used Framingham Risk Score, are inaccurate for individual risk prediction, as they tend to under- or overestimate patient's cardiovascular risk (58). The combination of imaging biomarkers with well established clinical parameters might improve personalized cardiovascular risk prediction. Individual plaque features, the extent and severity of atherosclerotic plaque burden were therefore introduced in risk prediction models (59,60). It has been suggested that total atherosclerotic plaque burden is even a stronger predictor of coronary events than total ischemic burden (61).

Histopathological investigations revealed that most acute coronary events originate from sudden atherosclerotic plaque rupture, while plaque erosions and calcified nodules represent the underlying morphology in the remaining cases (62-64). Plaque rupture is triggered by the acute disruption of the fibrotic cap that separates the necrotic plaque core from the blood stream (65). The necrotic plaque is highly thrombogenic and in the presence of pro-thrombotic factors in the blood stream it can lead to sudden thrombus formation with subsequent luminal obstruction. Intraluminal thrombus formation hinders adequate blood supply of the myocardium leading to acute myocardial infarction. Acute myocardial infarction represents the first clinical manifestation of CAD in majority of cases. Therefore, the early identification of high-risk asymptomatic patients is highly desirable although challenging with current techniques (66-68). The vulnerable plaque is a probability concept and it originates from the quest for finding important links between risk for coronary thrombosis and underlying plaque morphology (69,70). The morphological differences between the stable and unstable plaques might represent novel imaging targets for coronary CTA to identify these lesions (71). Compelling evidence suggests that certain adverse plaque characteristics visualized by coronary CTA are associated with acute coronary events (22,72). Thin cap fibroatheromas (TCFA) are considered as the precursor lesion of ruptured plaques based on intracoronary imaging studies and histological examinations. Pathological investigations revealed that the necrotic core of the vulnerable plaque has mean length of 8 mm and area of greater than

1.0 mm^2 in more than 80 % of the cases (65). Importantly, the large plaque dimensions of TCFA are above the spatial resolution of modern CT scanners, which provide unique opportunity for high-risk plaque detection. Based on prior studies, vulnerable plaques are most frequently located in the proximal and middle segments of the coronaries (22).

The thin fibrous cap represents a vulnerable interface between blood flow and lipid rich plaque content. In ruptured plaques the mean cap thickness of 23 ± 19 μm was reported and the vast majority of caps (95%) had a thickness below <65 μm (73). The visualization of fibrous cap on CT images is not feasible with current scanner technology due to the limited spatial resolution. However, beyond thin fibrous cap the identification of large necrotic core is one of the best discriminator between vulnerable and stable coronary lesions (74). Positive or outward remodeling represents another important vulnerability marker. The remodeling index is calculated as the vessel cross-sectional area at the site of maximal stenosis divided by the average of proximal and distal reference segments' cross-sectional areas (75). A remodeling index of ≥1.1 has been suggested as the threshold of positive remodeling in coronary CTA (22). In prior studies, the presence of positive remodeling and low-attenuation plaques on coronary CTA was associated with higher risk for developing acute coronary syndrome (ACS) (72). Low attenuation plaques were more frequent in patients presenting with ACS than with stable angina pectoris (79 vs 9 %; $p<0.0001$) (76).

The qualitative assessment of attenuation patterns in non-calcified plaques provides a new, more practical approach for plaque characterization independent of Hounsfield Unit (HU) value measurement. The napkin-ring sign (NRS) can be defined by the joint presence of distinct morphological features in non-calcified or partially calcified plaques: the plaque center of low CT attenuation apparently in contact with the lumen, and a ring-like annular pattern surrounding the core structure with higher attenuation values (77). NRS plaques have significantly larger necrotic core area than non NRS lesions (median of 1.10 vs 0.46 mm^2, respectively, $p = 0.05$) (78). NRS is a specific imaging biomarker for the detection of TCFA, and the identification of advanced lesions was significantly improved by the implementation plaque attenuation pattern classification as compared to conventional classification scheme (77). According to a recently published study, the napkin ring sign is an independent predictor of acute coronary syndrome (79).

DOI:10.14753/SE.2017.2079

Lipid rich, unstable plaques frequently contain calcium deposits of various sizes. Small (under 3 mm of diameter) calcific nodules, which are surrounded by non-calcified plaque tissue are termed as spotty calcifications (72,76). Motoyama et al. found, that spotty calcification had significantly higher prevalence in ACS as compared to lesions in stable angina patients [69]. Histological investigations demonstrated that microscopic calcification appears frequently in unstable plaques, however, it cannot be visualized with current CT technology due the limited spatial resolution. High-risk plaque features on CT are shown on **Figure 6.**

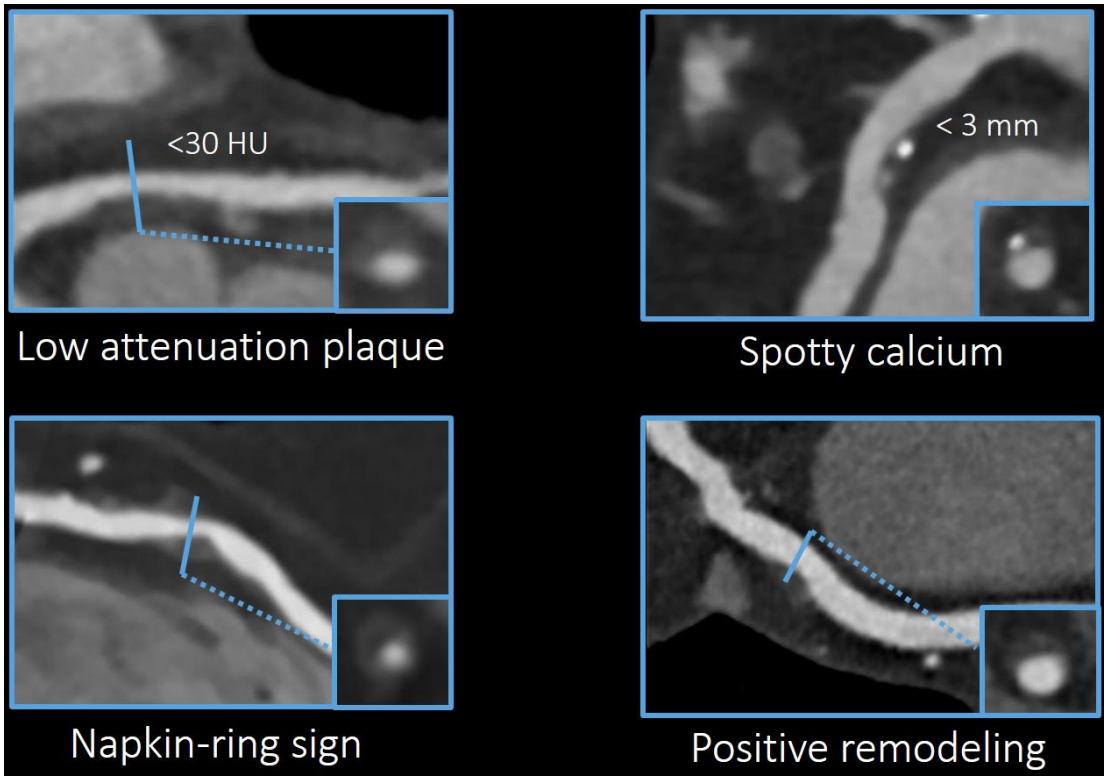

Figure 6. High-risk plaque features in coronary imaging *(own material).*
CTA images show the high-risk plaque features that were linked to adverse events. Vulnerable plaque features are more frequently found in ACS patients as compared to stable ones. HU: Hounsfield Units

The total coronary plaque burden can be described semi-quantitatively by the number of segments containing any coronary atherosclerotic plaque (segment involvement score) (80). Both obstructive (Hazard Ratio 2.60, 95 % CI 1.94–3.49, $p < 0.0001$) and non-obstructive CAD (Hazard Ratio 1.60, 95 % CI 1.18–2.16, $p = 0.002$) was associated with increased mortality rates, while patients without CAD had very favorable survival according to a risk adjusted analysis of Min et al. (81). Segment involvement by any non-obstructive plaque had independent prognostic value for clinical outcomes: highest risk was associated with non-obstructive CAD in the three main vessels (Hazard Ratio 4.75, 95 % CI 2.10–10.75, $p = 0.0002$) or involving ≥5 segments (Hazard Ratio 5.12, 95 % CI 2.16–12.10, $p = 0.0002$) during a 3-year follow up (82). A sub-analysis of the Clinical Outcomes Utilizing Revascularization and Aggressive Drug Evaluation (COURAGE) study has revealed that plaque burden based on ICA was a stronger predictor than ischemic burden for adverse cardiac events. Surprisingly, the extent of anatomic burden predicted adverse events (Odds Ratio 1.05, 95 % CI 1.02–1.09; $p < 0.001$), whereas the increase in ischemic burden (Odds Ratio 1.01, 95 % CI 0.98–1.04, $p = 0.54$) did not influenced clinical outcomes (61).

Coronary plaque burden assessment might also guide secondary preventive therapies. Statin eligibility based on CTA findings could provide a more adequate preventive therapy. In a recently published study Bittencourt et al. compared the cardiovascular risk in patient cohorts with different plaque burden categories as assessed by coronary CTA. Based on the number of coronary segments containing plaque, patients were classified as having extensive (≥4 segments) and non-extensive (<4 segments) CAD (83). The patients with non-obstructive but extensive CAD have similar adverse event rates (Hazard Ratio 3.1, 95 % CI 1.5–6.4) as patients with non-extensive obstructive CAD (Hazard Ratio 3.0; 95 % CI 1.3–6.9) during the nearly 4-year follow-up period. A different approach to coronary plaque burden assessment focusing on the role of non-obstructive plaques is desired as shown by the results of the multicenter CONFIRM study (84). The multicenter registry evaluated a total of 15187 patients without known CAD who underwent coronary CTA and demonstrated that non-obstructive CAD is an important predictor of mortality. Also, CT adapted Leaman score was introduced to quantify atherosclerotic burden based on coronary CTA images. The Leaman score incorporates lesion localization, degree of stenosis and plaque types and proved to be an independent, long-term prognostic tool of

hard cardiac endpoints. Weighting factors for the calculation of CT adapted Leaman score are shown in **Table 1** (85). Interestingly, patients with nonobstructive CAD and high Leaman score had similar outcomes as patients with obstructive CAD (86). The results of the PROMISE (Prospective Multicenter Imaging Study for Evaluation of Chest Pain) trial have shown that the assessment of non-obstructive CAD by CT is superior to functional testing and also provides important prognostic value in patients with stable chest pain (87).

DOI:10.14753/SE.2017.2079

Table 1. CT adapted Leaman score based on de Araujo Gonclaves et al. with weighting factors (85). Obstructive CAD was denifed as ≥50 % stenosis. PL: posterolateral branch, na: non-applicable,

Segment	Right dominance	Left dominance	Balanced
Coronary segments			
RCA proximal	1	0	0.5
RCA mid	1	0	0.5
RCA distal	1	0	0.5
PDA	1	na	0.5
Left main	5	6	5.5
LAD proximal	3.5	3.5	3.5
LAD mid	2.5	2.5	2.5
LAD distal	1	1	1
1st diagonal	1	1	1
2nd diagonal	0.5	0.5	0.5
LCX proximal	1.5	2.5	2.0
1st obtuse marginal	1	1	1
LCX distal	0.5	1.5	1
2nd obtuse marginal	1	1	1
PDA from LCX	na	1	na
PL branch from LCX	na	0.5	0.5
PL branch from RCA	0.5	na	na
Intermediate branch	1	1	1
Stenosis severity			
Obstructive CAD	1		
Nonobstructive CAD	0.615		
Plaque composition			
Non-calcified or mixed	1.5		
Calcified	1		

1.5 Qualitative and quantitative plaque assessment

Coronary CTA is an excellent noninvasive tool for the evaluation of coronary arteries that has been utilized widely in recent years. Coronary CTA allows a robust and non-invasive assessment of coronary plaques with regards to the quantification of plaque volumes and attenuation based characterisation of plaque components. Volumetric plaque assessment is based on lumen and vessel wall contouring and components are analysed using fixed or adaptive threshold settings for HU attenuation values (25). Fixed threshold setting utilizes preselected HU ranges as defined by the reader, whereas adaptive threshold setting is automatically defined by software applications based on e.g. the intraluminal contrast attenuation (88). Quantified total plaque volume has been proposed as a promising tool for risk prediction (89,90). Based on the CT numbers we can further differentiate noncalcified plaque components that are corresponding to necrotic core, fibro-fatty or fibrous plaque components using semi-automated software tools (**Figure 7**). It has been demonstrated that higher attenuation plaques correspond to predominantly fibrous plaques on Virtual-Histology Intravascular Ultrasound (VH-IVUS). On the other hand, plaques with <30 HU density showed a good correlation with VH-IVUS lipid rich plaques. However, the differentiation between lipid rich and fibrous lesions represents a major challenge for non-invasive imaging (91,92).

Semi-automated software tools were used in prior studies to investigate changes in plaque morphology and progression or regression of lesion severity. Lehman et al. sought to investigate alterations in plaque volume and composition over time among patients with acute chest pain (93). Utilizing reproducible semi-quantitative assessment they demonstrated a significant plaque burden and non-calcified plaque progression, which was associated with the clinical risk factors. Papadopoulou et al. analyzed the changes in coronary plaque burden, lumen dimensions, and arterial remodeling using serial imaging (94). Their results indicate that despite medical treatment atheroma size in non-culprit lesions increased by a simultaneous increase in the vessel size (positive remodeling). Quantitative plaque assessment requires extensive reading experience therefore, it is vulnerable to potential measurement errors. High intra- and inter-reader reproducibility was described for plaque and vessel dimensions, however, lower agreement was observed in compositional parameters (95). Versteylen et al. also found high intra- and inter-

observer correlations in total plaque volume (90). Semi-automated plaque quantification requires time consuming manual correction of the vessel and lumen contours. Recently, commercial software algorithms have been developed to overcome this challenge and achieve accurate plaque quantification with reduced analysis time.

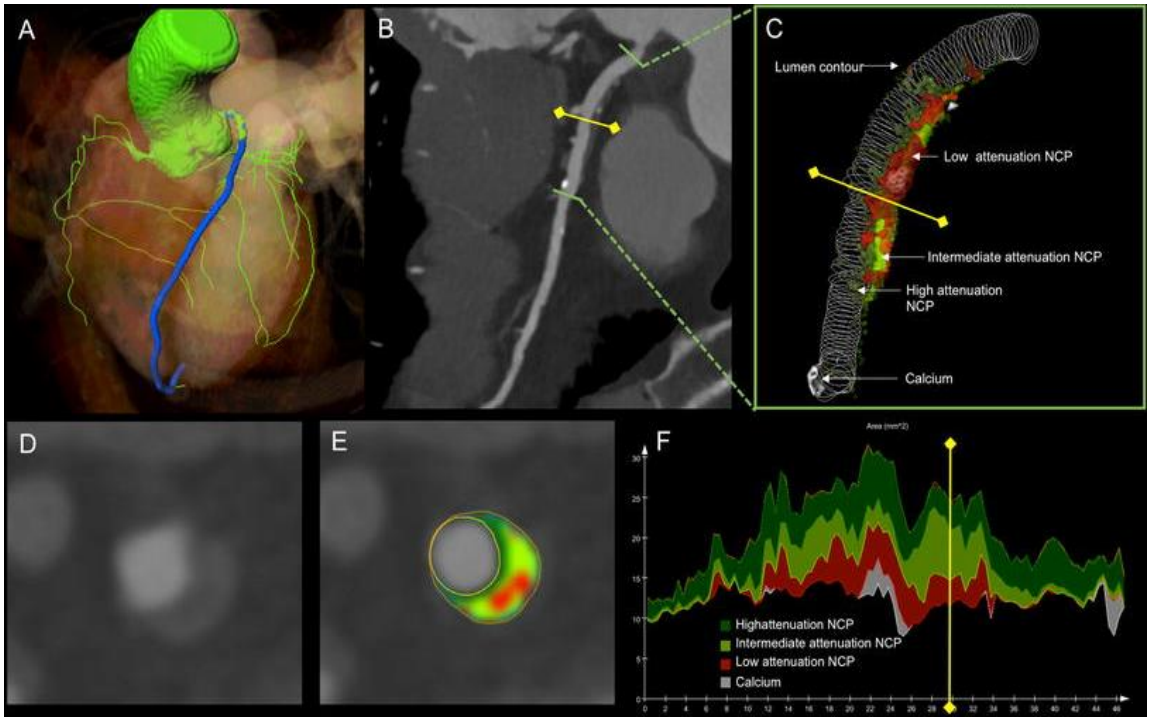

Figure 7. Semi-automated plaque assessment on CTA images (91).

A: representative case of semi-automated coronary plaque quantification and characterization showing a high-risk plaque on coronary CTA images reconstructed by iterative model reconstruction technique. a Coronary tree segmentation with centerlines (green). The LAD is indicated in blue. B: Curved multi-planar reconstruction of the left anterior descending coronary artery showing a high-risk plaque on the proximal segment. Green lines represent the boundaries of the analyzed segment, while the yellow line with squares at both ends illustrates the cross-sectional position of D and E panels. C: Volumetric assessment shows the contour of the lumen and the various plaque components based on CT attenuation with adaptive threshold settings. Low attenuation NCP components are shown in red, intermediate and high attenuation NCP components are shown in light and dark green, respectively. Calcium is indicated in white. D: Cross-sectional image showing a non-calcified, positively remodeled plaque with napkin-ring

sign. E: Plaque cross-section with colour overlay. F: Areas of different plaque components of the analyzed segment, y axis represents the area in mm^2, x axis the distance from the proximal end of the lesion (91). NCP: non-calcified plaque

The characterization of plaque components based on CT density values is feasible, although the differentiation between lipid-rich and fibrous components remains challenging. It has been suggested that the use of semi-automated analysis of plaque composition improves the differentiation of lipid-rich and fibrous plaques (96). Prior investigations described significant differences between relative volumes of lipid and fibrous plaques based on quantitative analysis. Plaque quantification based on CTA images demonstrated excellent correlation with VH-IVUS regarding vessel, lumen and plaque volumes as well as coronary stenosis (97). Furthermore, Rief et al. assessed the diagnostic performance of computer-aided CAD detection in coronary CTA using conventional coronary angiography as reference standard (98). The diagnostic performance of the computer-aided CAD detection was comparable with a less experienced reader, however it was substantially lower as compared to more experienced readers. Importantly, excellent image quality is a prerequisite for accurate plaque measurements using automated or semi-automated plaque quantification softwares.

Due to the latest advancements in image reconstruction and computing hardware, iterative reconstruction techniques were introduced by all vendors in the clinical setting to reduce image noise and radiation exposure (99). Concerns have been raised, that the impact of IR not only affects image quality but might influence plaque characterization. Studies suggest however, that hybrid-type IR significantly improves image quality as compared to traditional FBP algorithm without significantly altering coronary plaque analysis (100,101). Moreover, the utilization of model based IR algorithm improves the feasibility of automated plaque assessment with coronary CTA, because it requires less vessel-wall boundary corrections compared to other reconstruction techniques based on an ex vivo study (102).

1.6 Novel iterative reconstruction algorithms in coronary imaging

Interpetation of CAD on coronary CTA images is mainly influenced by image quality. Common artifacts of CTA images are image noise with poor signal-to-noise ratio (SNR), so called blooming artifacts due to stents or calcification and motion artifacts (103). Most coronary CTA studies have been reconstructed with noise prone filtered back projection (FBP). FBP is a fast and robust technique that has been widely utilized in CT imaging. Ever growing number of cardiac diagnostic tests necessitates effective reduction of radiation exposure (36,104). With hardware evolution various computationally intense iterative image reconstruction techniques have been introduced by all vendors in order to reduce radiation exposure of cardiac CT while maintaining or even improving SNR **(Figure 8)** (105).

Using traditional FBP reconstruction CT images are generated from the raw data under certain assumptions about scanner geometry. Full IR provides complex modelling of noise distribution and scanner geometry and the process consists of forward and backward reconstruction steps using the images and the projection data to improve image quality. Different number of iteration steps can be applied and whenever projection data is reconstructed back to images corrections are made. These corrections aim to optimize images and reduce image noise by taking CT system characteristics into consideration using artefact and noise reducing models. IR techniques iterate in either image and raw data domain or both. Hybrid iterative reconstruction (HIR, Philips Healthcare, Best, The Netherlands) utilizes statistic-model based denoising both in raw and image domains, providing up to 55% noise reduction for cardiac image acquisition at standard tube settings (106,107). Moreover, two recent studies demonstrated that HIR had no significant effect on plaque morphology assessment (108-112).

DOI:10.14753/SE.2017.2079

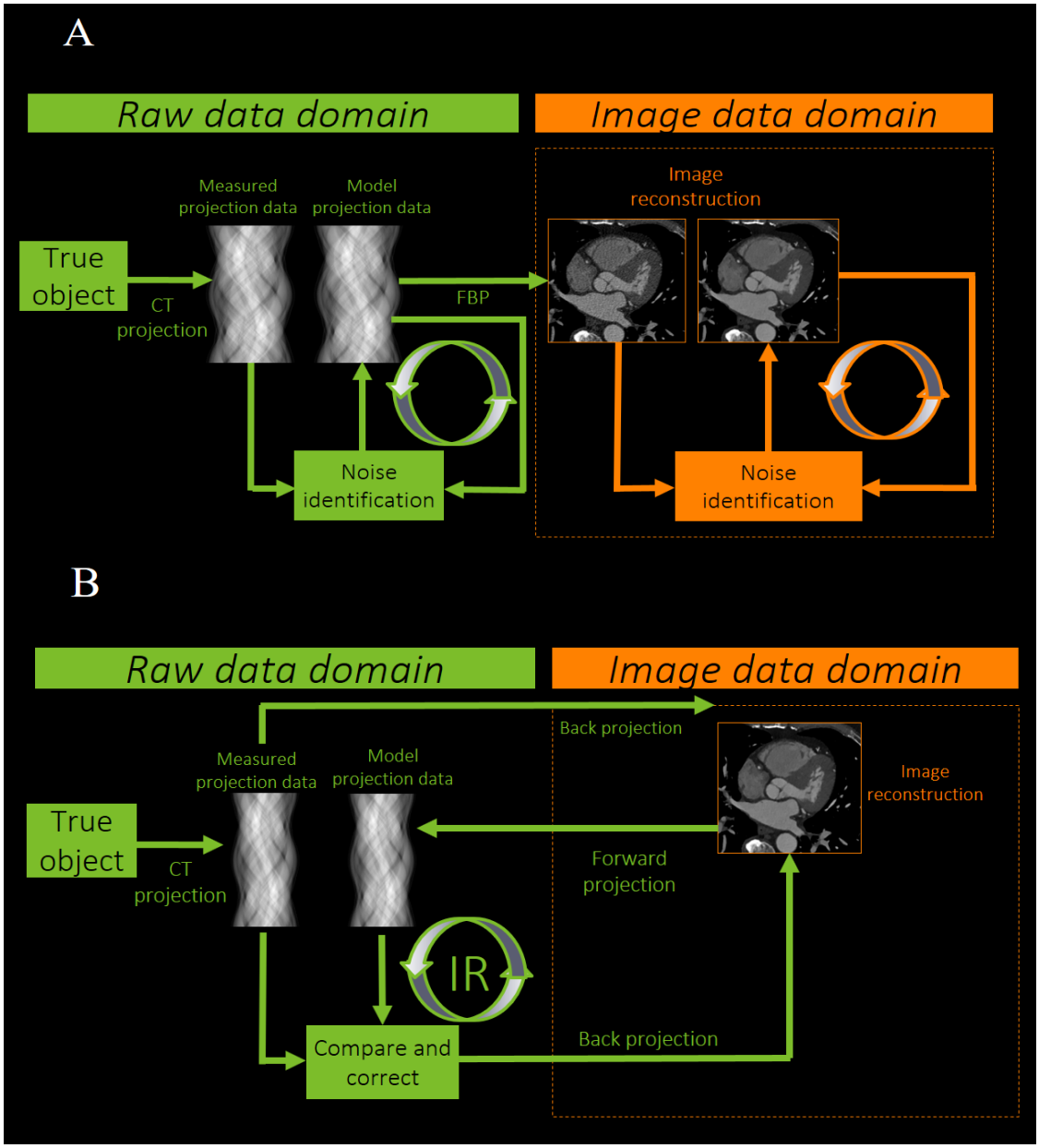

Figure 8. Technical principles for iterative reconstruction algorithms (modified after *Willemink MJ et al. Eur Rad (2013)* (113,114).

Traditional FBP is a widely applied analytic reconstruction algorithm that assumes that the acquired projection data are free of noise. Iterations can be performed in either the raw data or image data domain, or both. Hybrid-type (Panel A) IR applies noise reduction algorithms implemented in conjunction with a back projection reconstruction process. Novel model based IR (Panel B) also accounts for system geometry (focal spot size, shape of X-ray beam, interactions of emitted photons with tissue and detector) and iterate images in the raw data domain.

The impact of IR techniques on image quality and its potential to reduce radiation exposure of patients has been investigated in several recent studies (115).

Model based type of image reconstructions represents the latest advancement among image reconstruction techniques that showed improved image quality and holds the potential for further dose reduction (116). Three-dimensional raw data based reconstruction techniques were introduced with forward modeling of recognizing system geometry (focal spot size, shape of X-ray beam, interactions of emitted photons with tissue and detector) additionally to statistical modeling (115). Preliminary data showed the potential of model based IR techniques to achieve more robust noise reduction and/or improved image quality of coronary CTA **(Figure 9)**.

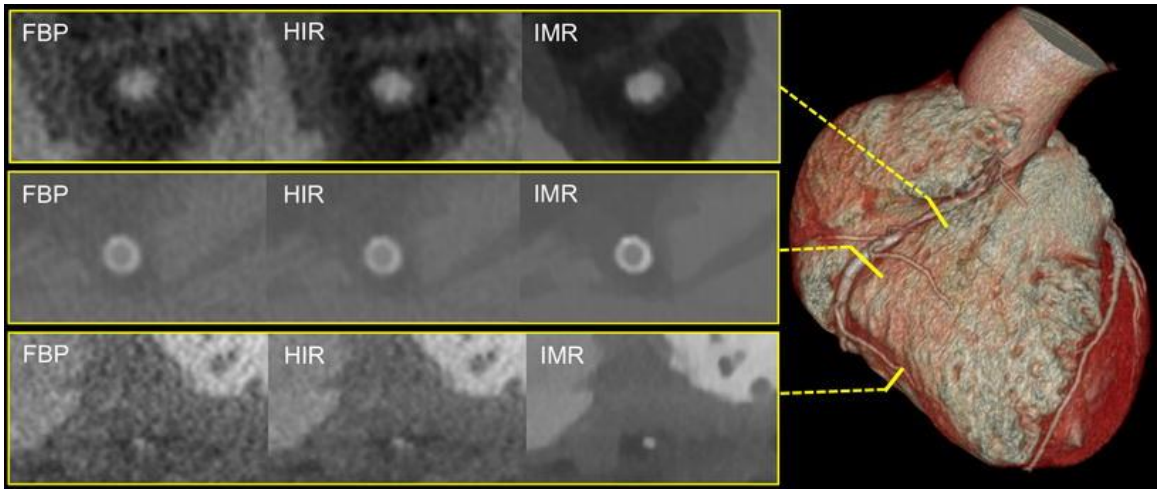

Figure 9. Image quality comparison between traditional FBP reconstruction and novel IR techniques (91).

The figure illustrates the image quality of coronary CTA reconstructed with FBP, HIR and IMR. The volume rendered image illustrates the locations of coronary artery cross-sections depicted in the yellow panels. The upper panel shows the proximal segment of the RCA. IMR provides superior image quality as compared to FBP and HIR, allowing a better delineation of the coronary lesion. The middle panel represents a stent cross-section in the mid-RCA. Due to the reduced noise level it is easier to evaluate the stent by using IR techniques. The lower panel represents a cross-section from the posterior descending coronary artery. Again, the abundant noise in FBP hinders the evaluation of the coronary artery with small diameter (91).

DOI:10.14753/SE.2017.2079

2. OBJECTIVES

2.1 Defining the impact of iterative reconstruction on calcium score and risk assessment

Despite the widespread use of novel reconstruction techniques the model based IR techniques have not yet been validated for coronary calcification measurements in clinical setting. We sought to assess the impact of iterative model reconstruction on coronary artery calcium quantification as compared to the standard FBP algorithm and HIR. In addition, we aimed to simulate the impact of IR on CAC score based risk stratification of an asymptomatic patient population.

2.2 Defining the influence of iterative reconstruction on image quality

Excellent image quality is the prerequsite of accurate plaque assessment and thus patient management. Advancements in image reconstruction techniques hold the potential to provide better visualisation of coronary arteries by improving image quality. We aimed to further elucidate the impact of novel IR techniques (HIR and IMR) as compared to FBP on subjective and objective image quality for coronary artery analysis. Comprehensive quantitative image quality analysis included signal- and contrast-to-noise calculations for proximal and distal coronary segments, whereas qualitative analysis aimed to evaluate the effects of IR on vessel sharpness and image noise on visual assessment.

2.3 Defining the changes in plaque quantification using iterative reconstruction

There is a growing body of evidence regarding the prognostic value of quantified coronary plaque volume for adverse events. We aimed to assess the impact of IMR on calcified plaque quantification as compared to FBP and HIR in coronary CTA. We hypothesize that novel model based IR could influence measured plaque volumes that ultimately influence individual risk assessment.

DOI:10.14753/SE.2017.2079

3. METHODS

3.1 Study design and study population for CAC based risk assessment

In a single center study, we performed CAC scoring in two distinct patient cohorts to evaluate the effects of novel IR methods. We enrolled and evaluated 63 symptomatic patients referred to clinically indicated cardiac CT examination due to suspected coronary artery disease. On the basis of CAC score differences observed in the study population we subsequently simulated the effect of IR on the risk stratification in an asymptomatic test population of 504 individuals. The test population is part of a National Health Examination survey, which is a population-based cardiovascular screening program (117). The population of a suburban town with 8000 adult inhabitants (age ≥ 20 years) were invited to this voluntary screening campaign between 2012 and 2014. The protocol included a comprehensive health interview survey, and examination survey with cardiac ultrasound, carotid intima-media-thickness, ECG and CAC scoring. Patients with known coronary artery disease and patients with irregular heart rate were excluded from this study. Baseline characteristics of the two patient cohorts are summarized in **Table 2**. The institutional ethics review board has approved our study and participants provided written informed consent.

DOI:10.14753/SE.2017.2079

3.1.1 Coronary CT data acquisition and image analysis

All patients were scanned using a 256-slice CT-scanner (Brilliance iCT, Philips Healthcare, Best, The Netherlands). Oral beta-blockers were administered, if the heart rate exceeded 65 bpm. Non-contrast ECG-gated scans were acquired with prospective triggering at 78% of the RR-interval for CAC scanning using the following acquisition parameters: 128 mm × 0.625 mm collimation, 270 ms tube rotation time, 120 kV tube voltage, 30 mAs tube current.

We reconstructed axial images with 3 mm slice thickness using standard FBP, HIR (iDose4, Philips Healthcare, Cleveland, OH, USA) and IMR (IMR, Philips Healthcare, Cleveland, OH, USA) algorhitms. The vendor provides 1–7 levels for HIR and 1–3 levels for IMR noise reduction, we applied a medium level for both HIR (Level 4) and IMR (Level 2) technique. All images were reconstructed usind a single workstation (Extended Brilliance Workspace, Philips Healthcare, Best, The Netherlands), resulting in 3 datasets for each patient. Dose length product (DLP) of every examination was calculated and registered in an online database along with anamnestic and clinical parameters. To estimate effective radiation dose, the DLP was converted into millisieverts by multiplying it by a body region-specific scaling factor (k-factor = 0.014) [16]. Image noise was defined as the standard deviation of the CT attenuation values in a region of interest (ROI) placed in the aortic root. Identical 2 cm^2 large ROIs were placed in the level of the left main coronary artery.

We performed CAC scoring on the axial images using a commercially available software application (Heartbeat-CS, Philips Healthcare, Best, The Netherlands) according the Agatston-method (19). The software identified the coronary artery plaques with an area of $\geq 1 mm^2$ and a density of greater than 130 Hounsfield Units (HU). Subsequently coronary plaques were selected manually by the first observer (with 5 years of experience in cardiac CT) which allowed the semiautomatic software to calculate CAC scores. The software also automatically calculates area and volume for coronary lesions. All three reconstructions (FBP 3 mm, HIR 3 mm, IMR 3 mm) for all patients were assessed in a random fashion. In addition datasets of 20 randomly selected patients were assessed two times by a second observer (with 6 years of experience in cardiac CT) for calculating inter- and intra-observer variability. Patients were classified into the following risk

categories based on the CAC score values: 0 normal/no risk, 1–10 low, 11–99 low-intermediate, 100–399 intermediate, 400 < high risk (48).

3.1.2 Risk reclassification in the test patient cohort

In order to assess the effect of the different reconstruction techniques on risk stratification we implemented the reclassification rates derived from the study population to the larger test population. First, we calculated the differences in total CAC score values between the different reconstruction methods. Second, relative differences were calculated by dividing the average difference of two reconstructions by the average of the minuend's total CAC score. Using the relative differences calculated on the study population, we multiplied the total CAC of the original 3mm FBP scores by the relative differences to get simulated HIR and IMR results on a patient basis. With using the simulated HIR and IMR calcium score values we determined how many patients shifted from one risk group to another. Reclassification ratio was calculated by dividing the number of people who shifted from a given risk group by the total test population.

DOI:10.14753/SE.2017.2079

3.2 Study design and population for image quality and plaque analysis

In a single center study, we enrolled 52 consecutive individuals who underwent routine clinical coronary CTA examination due to suspected CAD. Patients who had calcified and/or partially calcified plaque were included in the further analysis to study the effects of IR on plaque characteristics. As we used automated plaque quantification, partially calcified lesions were not further distinguished to predominantly non-calcified or predominantly calcified plaque types. Patients with previous bypass surgery or coronary stent implantation were excluded from the analysis. To minimize the impact of motion artifact on image quality, patients with arrhythmia and/or with a heart rate of ≥65 beat per minute were also excluded. Informed consent was waived by the institutional review board due to the retrospective design of the study. No additional data acquisition was performed in addition to routine care CTA examinations.

DOI:10.14753/SE.2017.2079

3.2.1 Scan protocol

All examinations were performed with a 256-slice scanner (Brilliance iCT 256, Philips Healthcare, Best, The Netherlands) with prospective ECG-triggering. Images were acquired in cranio-caudal direction during a single breath-hold in inspiration using the following imaging parameters: 128×0.625 mm detector collimation, 270 ms gantry rotation time, 120 kV tube voltage and 300 mAs tube current, field-of-view of 18 cm with a matrix of 512×512. We acquired images during the most quiescent mid-diastolic period with 3% padding. Iomeprol contrast media with an iodine concentration of 400 mg/ml (Iomeron 400, Bracco Ltd, Milan, Italy) was injected into an antecubital vein via an 18-gauge catheter and dual-syringe system. A triphasic injection protocol with 90–95 ml contrast agent was applied at a flow rate of 5.0-5.5 ml/s. We used bolus tracking technique with an ROI placed in the left atrium for proper scan timing.

All coronary CTA images were reconstructed with FBP, HIR and IMR on a dedicated workstation. We reconstructed all images with 0.8 mm slice thickness, 0.4 mm increment and medium cardiac kernel and applied a medium level for HIR (level 4 of 1–7) and IMR (level 2 of 1–3).

DOI:10.14753/SE.2017.2079

3.2.2 Qualitative and quantitative image quality analysis

We used a four point Likert-scale to analyze and classify subjective image quality parameters on axial slices **(Figure 10)** (118). Overall image quality was defined as a summary of image sharpness, image noise and blooming artifacts, if present and categorized as follows: non-diagnostic (0); moderate, considerable artifacts with diagnostic image quality (1); good, minor artifacts (2) and excellent (3) image quality. Subjective noise was further analyzed and rated according to the graininess on the coronary CTA image: severe image noise (0); above average (1); average (2); no image noise (3).

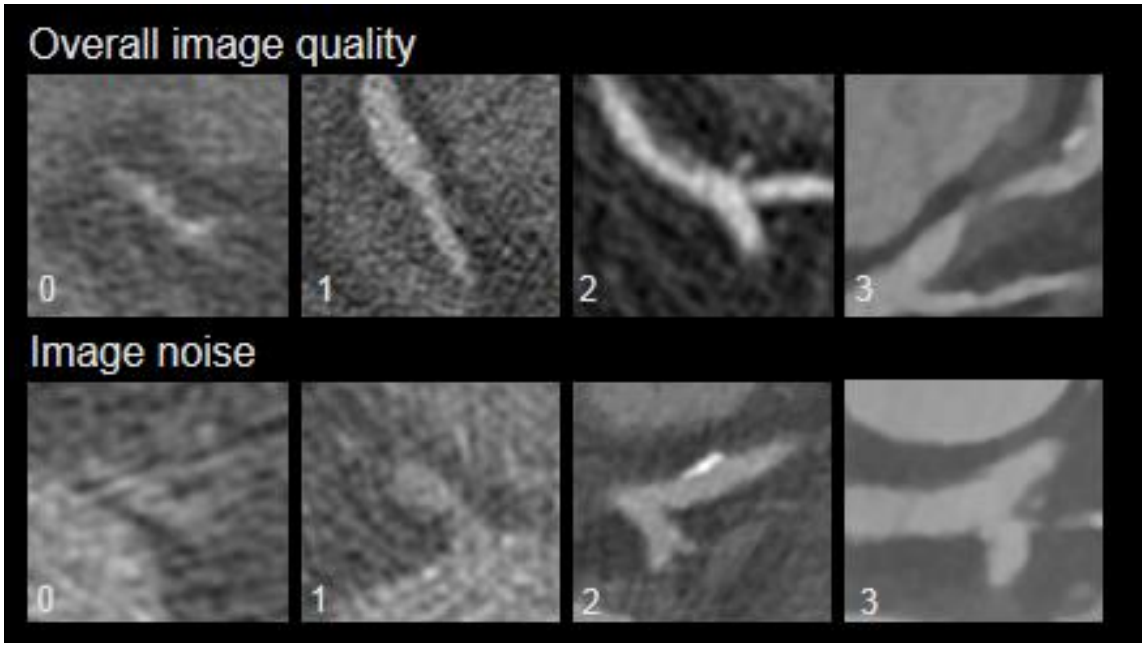

Figure 10. Qualitative image quality analysis for overall image quality and image noise using a 4-point Likert scale *(own material)*.

DOI:10.14753/SE.2017.2079

On quantitative analysis, proximal and distal segments of the left anterior descending artery, circumflex artery and right coronary artery were evaluated. As we aimed to assess the differences between proximal and distal coronary segments, middle coronary segments and side branches were not included in our analysis. Circular regions of interest (3–4 mm^2) were manually placed in the coronary arteries and pericoronary fat to obtain median CT number in Hounsfield units. ROIs were placed in a homogenous region of the proximal and distal segments of LAD, CX and RCA and the correspondent areas of the pericoronary fat. Artifacts, inhomogeneous regions and plaques were carefully avoided. Median image noise was determined as the standard deviation (SD) of the CT attenuation placed a circular ROI (200 mm^2) within the aortic root at the level of the LM coronary ostium. The copy and paste function of the workstation was used to measure exactly the same ROIs at all three reconstruction datasets. **Figure 11** demonstrates the measurements for the aorta and the proximal LAD for all three reconstructions. Signal-to-noise ratio is defined as the CT attenuation value in a given segment divided by the image noise. Contrast to noise (CNR) ratios were calculated for all segments, as CNR = (HU_{lumen} – HU_{fat}) / image noise; HU_{lumen} and HU_{fat} represents the median CT attenuation in the coronary artery lumen and the pericoronary adipose tissue (119).

DOI:10.14753/SE.2017.2079

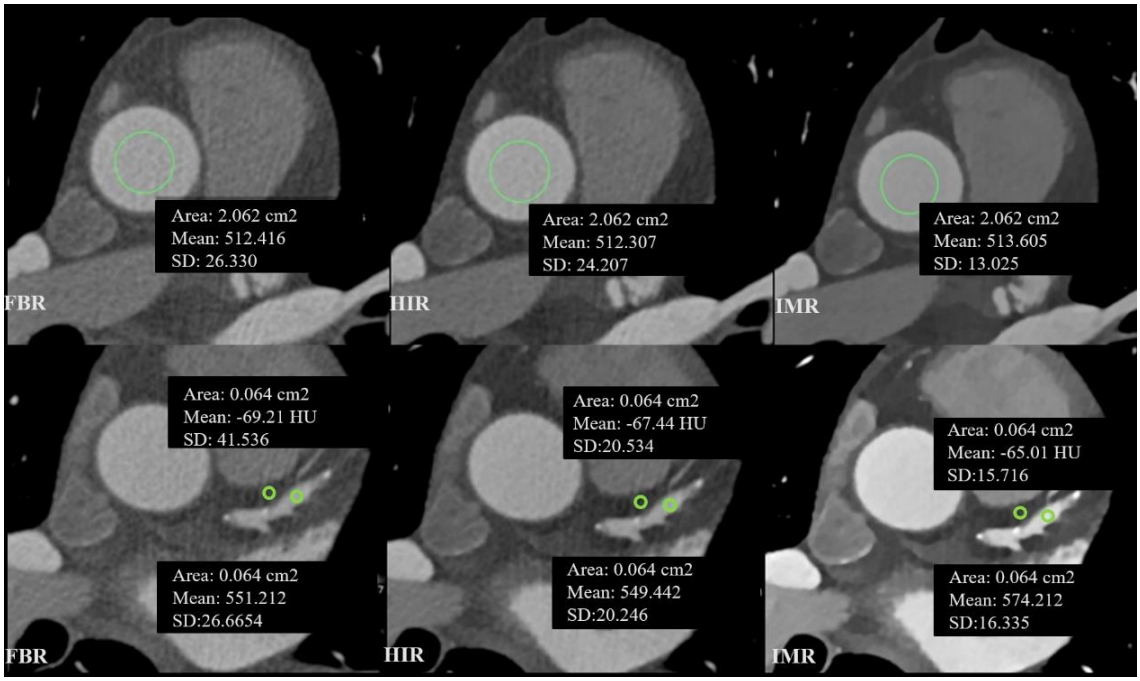

Figure 11. Quantitative image quality assessment on images reconstructed with FBP, HIR and IMR *(own material).*

Comparison of image quality across different reconstruction algorithms. On the upper row green circles represent measurements of image noise as defined by the standard deviation of HU in the aorta. Substantially lower standard deviation values (image noise) were detected using HIR and IMR as compared to FBP. We measured HU values in the given coronary segment and pericoronary fat to calculate SNR and CNR values.

HU: Hounsfield unit, SD: standard deviation.

3.3 Semi-automated plaque assessment

We performed semi-automated plaque characterization and quantification on the same study population as described in chapter 3.2. Scan protocol is also identical to the previously reported section (3.2.1).

We transferred the datasets present with any calcified or partially calcified plaque to a dedicated offline workstation (QAngio, version 2.1; Medis Medical Imaging Systems, Leiden, The Netherlands) for further plaque characterization **(Figure 12)**. For plaque quantification each dataset was loaded separately and after automated segmentation of the coronary tree the proximal and distal end points of each plaque were set manually. We took screen shots of anatomical fiducial markers to ensure that we analyzed the same plaques across the different reconstruction datasets. Fully automated plaque quantification was performed without any manual corrections of boundaries to exclude the influence of observer bias. After automated delineation of the outer and inner vessel-wall boundaries we used the following fixed thresholds: calcified plaque volumes (>130 HU), non-calcified plaque volumes with high attenuation (90–129 HU), intermediate attenuation (30–89 HU) and low attenuation (<30 HU) (25).

DOI:10.14753/SE.2017.2079

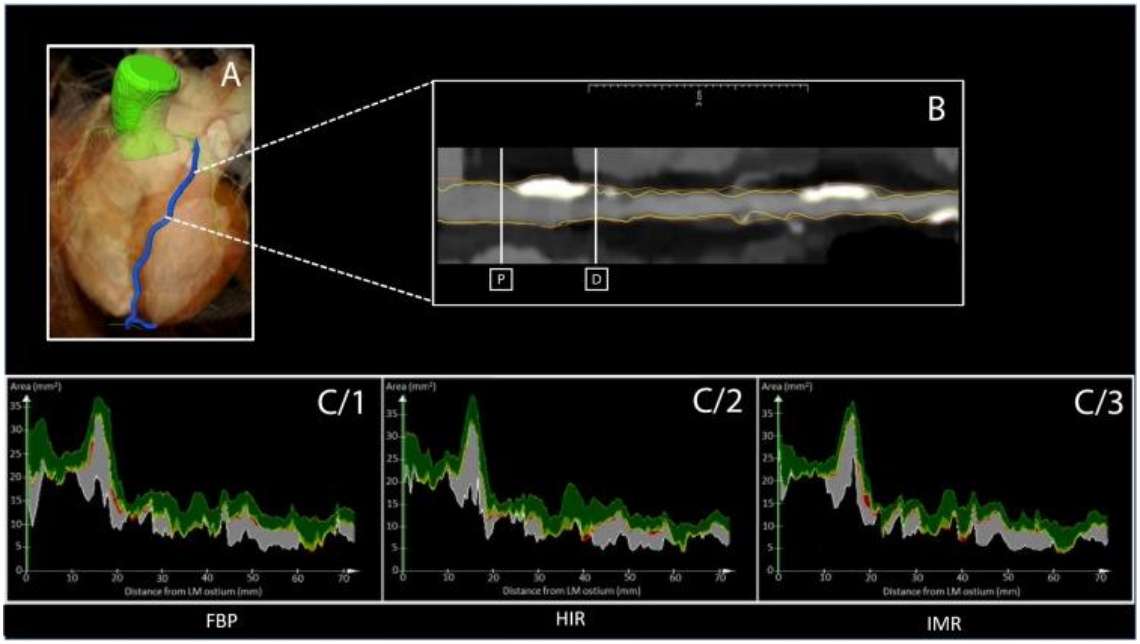

Figure 12. Plaque quantification with FBP, HIR and IMR technique (88).

Components of a mainly calcified atherosclerotic plaque in the proximal left anterior descending artery (LAD, marked with the blue line on the volumetric 3D reconstruction) are quantified using automated software after coronary segmentation (Panel A). Consequently, the proximal (P) and distal (D) endpoints of the predominantly calcified plaque were selected on the CT images (Panel B). After centerline extraction the software automatically detected lumen (yellow) and outer vessel wall (orange) contours. Panel C shows the plaque measurements for all three reconstructions (C/1: FBP; C/2: HIR; C/3: IMR) and the colors are indicated for various plaque components (white: calcified, >130 HU; dark green: non-calcified with high attenuation, 90–129 HU; light green: non-calcified with intermediate attenuation, 30–89 HU; red: non-calcified with low attenuation (<30 HU) Plaque volumes were 156.0 mm3 for FBP, 148.7 mm3 for HIR and 133.2 mm3 for IMR. Calcium volumes were 80.1 mm3 for FBP, 77.7 mm3 for HIR and 74.2 mm3 for IMR, respectively.

FBP: filtered back projection; HIR: hybrid iterative reconstruction; IMR: iterative model reconstruction, HU: Hounsfield units.

3.4 Statistical analyses

Continuous variables were presented as mean ± standard deviation or as medians with interquartile range as appropriate depending on the distribution of the values, whereas categorical variables were expressed as percentage. The Kolmogorov-Smirnov test was applied to evaluate normality of continuous variables. The inter- and intra-reader agreement between calcium measurements was calculated using Lin's concordance correlation coefficient. The following descriptive scale was used for values of the concordance correlation coefficient: <0.90 Poor, 0.90–0.95 Moderate, 0.95–0.99 Substantial, >0.99 Almost perfect. Our data was not normally distributed for CAC score, area and volume and therefore these parameters were compared by using the Friedman test using Bonferroni–Dunn test for post hoc multiple comparisons. Differences between the cohorts were evaluated with Mann–Whitney test for continuous parameters and Chi-square test for categorical parameters. Differences in risk stratification were also assessed using Chi-square test with Bonferroni correction.

The number of assessable segments for image quality analysis was compared using chi-square test. Plaque features and image quality parameters (both quantitative and qualitative) of the IMR, HIR, and FBP images were not normally distributed and were compared by using the Friedman test with Bonferroni-Dunn test for post-hoc comparisons. The Wilcoxon signed rank test was used to assess the difference between image quality parameters of the proximal and distal vessel segments. The inter-reader reproducibility between image quality measurements was calculated using Lin's concordance correlation coefficient. The reproducibility of visual assessment of two observers was measured with kappa statistics interpreted as follows: $\kappa < 0.20$ poor, 0.21–0.40 fair, 0.41–0.60 moderate, 0.61–0.80 good, 0.81–1.00 very good. Statistical analysis was performed using SPSS (IBM Corp, version 22.0, Armonk, NY, USA). A p value of ≤ 0.05 was considered statistically significant.

DOI:10.14753/SE.2017.2079

4. RESULTS

4.1 Calcium score based risk reclassification by novel iterative reconstruction algorithms

To define the effects of IR on calcium score based risk predictions we analyzed a total of 63 patients and performed a simulation on the test population of 504 individuals. Characteristics of the study and test population is summarized in **Table 2**.

The median values of CAC scores were 147.7 (IQR 9.6–582.9), 107.0 (IQR 5.9–526.6) and 115.1 (IQR 9.3–508.3) for FBP, HIR and IMR, respectively. The minimum CAC score value was 0, whereas the maximum total CAC value was 2347.3 on FBP. The relative differences compared to FBP were −7.2 % for HIR and −7.3 % for IMR. Post-hoc analysis showed a significant difference in calcium scores between images reconstructed with HIR and IMR as compared to FBP ($p < 0.001$). However, calcium scores of images reconstructed with HIR and IMR did not differ ($p = 0.86$). Image noise decreased significantly with the use of IR: 40.1 ± 12.9 with FBP, 26.5 ± 7.2 with HIR and 13.7 ± 3.4 with IMR ($p < 0.001$). Calcium area values were 86.4, 74.6 and 67.0 mm^2, while calcium volume values were 129.9, 112.2 and 100.8 mm^3 for FBP, HIR and IMR, respectively. Both area and volume values were significantly lower with HIR and IMR as compared to FBP ($p < 0.001$), however there was no significant difference between HIR and IMR reconstructions ($p = 1.000$).

DOI:10.14753/SE.2017.2079

Table 2. Patient characteristics of the study and test population.

BMI: body mass index; PAD: peripheral arterial disease; DLP: dose length product

Patient data	Study population (N=63)	Test population (N=504)	p value
Age (years)	60.1 ± 11.0	64.6 ± 10.3	0.002
BMI (kg/m^2)	28.3 ± 4.5	28.7 ± 5.0	0.970
Male gender, n (%)	37 (58.7)	211 (41.9)	0.011
Cardiovascular risk factors, n (%)			
Hypertension	45 (71.4)	295 (58.5)	0.009
Diabetes mellitus	12 (19.0)	82 (16.3)	0.334
Dyslipidemia	34 (54.0)	236 (46.9)	0.157
Smoking	28 (44.4)	197 (39.0)	0.212
PAD	6 (9.5)	36 (7.2)	0.319
Radiation dose			
DLP (mGy×cm)	31.8 ± 6.4	93.0 ± 28.2	<0.001
Effective dose (mSv)	0.45 ± 0.2	1.2 ± 0.5	<0.001

DOI:10.14753/SE.2017.2079

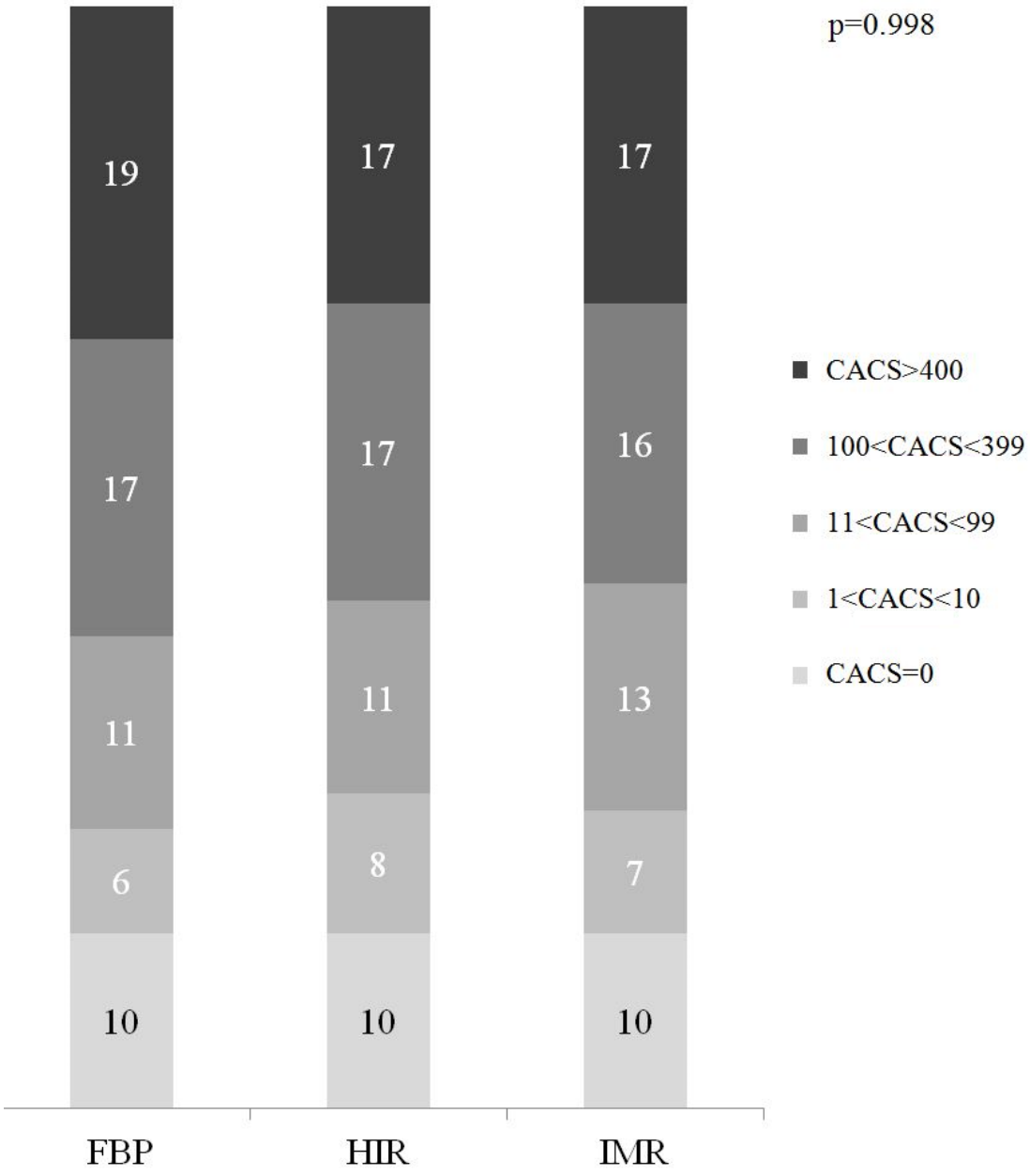

Figure 13. Coronary artery calcium score based risk categories of the study population (120). Minor changes were seen due to the utilization of HIR and IMR compared to FBP. CACS: Coronary artery calcium score; FBP: Filtered back projection; HIR: Hybrid iterative reconstruction; IMR: Iterative model reconstruction

As compared to FBP, the utilization of HIR and iterative model reconstruction resulted in a modest reclassification rate among the low and intermediate groups of the study population; 6 of 63 patients were reclassified using HIR algorithm as compared to FBP: 2 high-risk patients were moved to the intermediate group, while two patients with intermediate risk to the low-intermediate group and two patients with low-intermediate risk to low the risk group (**Figure 13**). The use of IMR also lead to reclassification of six patients as compared to FBP: 2 high-risk patients were moved to the intermediate group, whereas 3 intermediate risk patients were moved to the low-intermediate and 1 patient with low-intermediate risk was moved to the low-risk group. There was no significant difference between the three reconstruction techniques in risk categories ($p = 0.998$).

The median CAC scores of the test population with FBP was 22.3 (IQR 0–199.2) (range of 0–4549.2). The relative differences found in the study population were used to simulate the effect of HIR and IMR in the larger test patient cohort. Based on our simulation the extrapolation of relative differences obtained by iterative algorithms yielded 2.4 % (12 patients) change in risk stratification in 504 individuals **(Figure 14)**. Reclassification rate did not differ significantly among the 3 reconstructions ($p = 0.998$). All 12 patients were moved to lower risk groups based on their CAC values: 6 high-risk individuals were reclassified into intermediate group, and five patients were moved from the intermediate to low-intermediate category. Representative images are shown on **Figure 15** to demonstrate the effects of IR on image noise and calcium score values.

The inter-observer reproducibility of calcium scoring was substantial in images reconstructed with FBP (concordance correlation coefficient 0.973–0.986) and almost perfect reproducibility was found using IR techniques (HIR and IMR 0.990–0.997). Intra-observer correlation values were assessed in 20 patients with almost perfect concordance correlation coefficient values in all reconstructions (0.996–1).

DOI:10.14753/SE.2017.2079

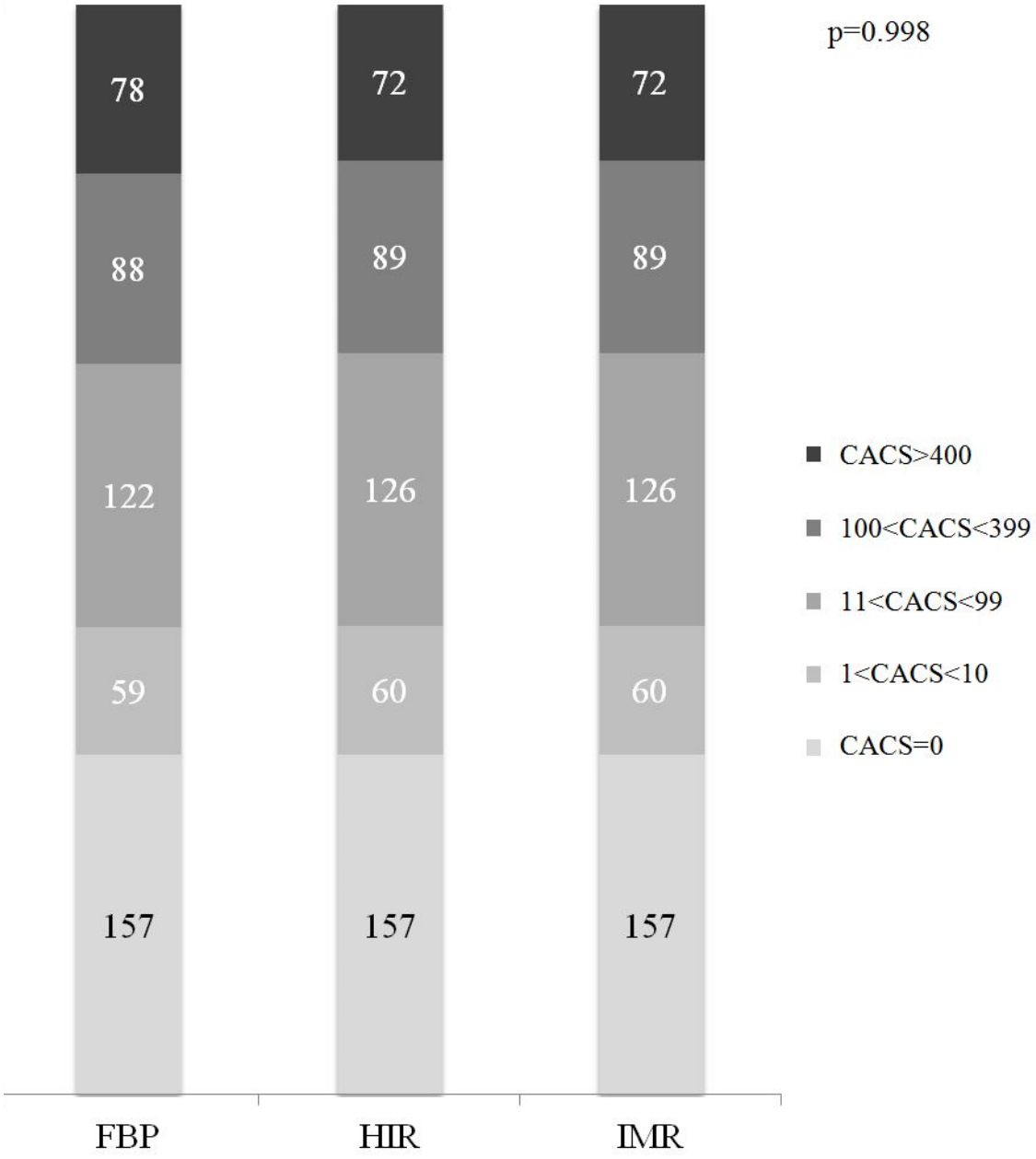

Figure 14. Risk reclassification based on CAC scores in the test population (120). Risk categories of the asymptomatic test population based on the CAC scores and the impact of HR and IMR. Based on our simulation, IR yielded a moderate reclassification rate of 2.4 % of 504 asymptomatic patients of a cardiovascular screening program. CACS: Coronary artery calcium score; FBP: Filtered back projection; HIR: Hybrid iterative reconstruction; IMR: Iterative model reconstruction

DOI:10.14753/SE.2017.2079

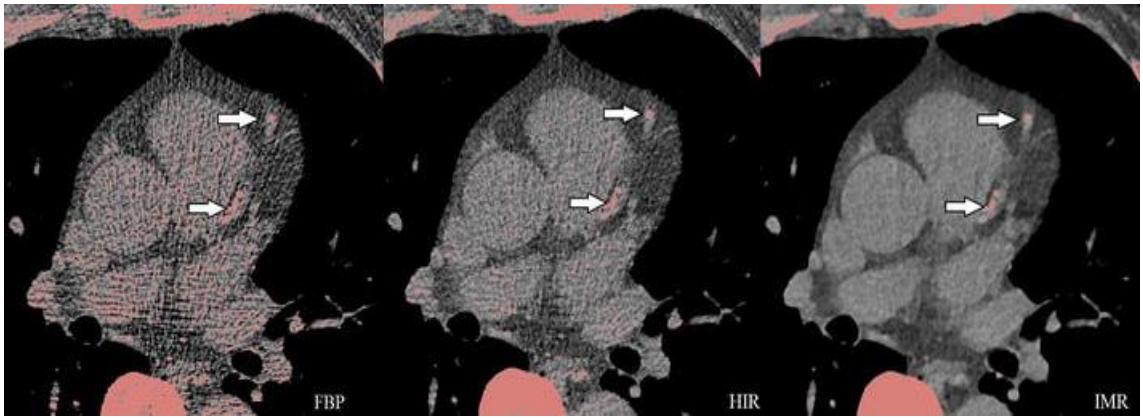

Figure 15. A representative case reconstructed with FBP, HIR and IMR (120).
Axial cardiac CT images with 3 different reconstruction techniques (FBP, HIR, IMR) at the level of the middle segment of the LAD. In this case calcified plaques are visible in the proximal and middle LAD segments (arrows). Calcified plaques are identified by dedicated semiautomatic software, however excessive noise seen on FBP image hinders CAC measurements. Total CAC scores were: 2377.6 for FPB, 2202.6 for HIR and 2137.3 for IMR.

DOI:10.14753/SE.2017.2079

4.2 Comparison of image quality parameters using different reconstructions

This study consisted of 52 patients who underwent coronary CTA at our institute. The image quality analysis included 468 triplets of coronary artery segments reconstructed with IMR, HIR and FBP. We identified 41 isolated calcified or partially calcified plaques; 25 plaques were located in the LAD, 10 plaques in the RCA, 5 in the LCX and 1 in the left main coronary artery. Patient characteristics are summarized in **Table 3.**

Qualitative image analysis showed diagnostic image quality (rated as 1–3) in 453 segments (96.8%) with IMR, 437 (93.4%) with HIR and 407 (87.0%) with FBP ($p < 0.01$). Overall subjective image quality significantly improved with the application of HIR as compared to FBP, and further improved with IMR ($p < 0.01$ all) **(Figure 16/A)**. IMR yielded lower image noise by qualitative assessment as compared to HIR and FBP ($p < 0.01$ all). The majority of the coronary segments were rated as having no image noise (395/468, 84.4%), or average image noise (73/468, 15.6%) in the datasets reconstructed with IMR technique **(Figure 16/B)**. The inter-reader reliability between the two readers was good for overall image quality (κ: 0.71), and image noise (κ: 0.73).

DOI:10.14753/SE.2017.2079

Table 3. Demographic characteristics and imaging parameters.

SD: standard deviation; IQR: interquartile range; BMI: body mass index; PAD: peripheral arterial disease; DLP: Dose Length Product

Parameters	N = 52
Age (years), median [IQR]	66.0 [59.0-71.8]
BMI (kg/m2), median [IQR]	27.5 [25.0-30.8]
Female gender, n (%)	13 (25)
Cardiovascular risk factors, n (%)	
Hypertension	41 (78.8)
Diabetes	9 (17.3)
Dyslipidemia	28 (53.8)
PAD	7 (13.5)
Stroke	5 (9.6)
Smoking	20 (38.5)
Prior use of beta blocker, n (%)	22 (42.3)
CTA characteristics, median [IQR]	
Contrast agent (ml)	95.0 [90.0-95.0]
DLP (mGy×cm)	308.0 [307.0-308.0]
Average heart rate (beats/min)	57.0 [52.0-60.0]

DOI:10.14753/SE.2017.2079

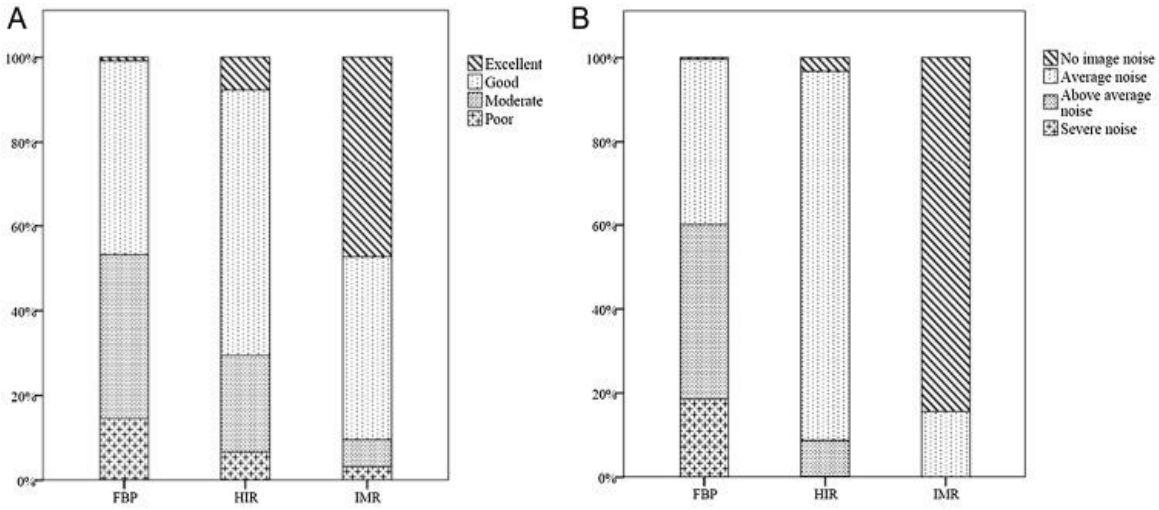

Figure 16. Visual assessment of image quality (88).

The use of IMR was associated with improved overall image quality (Panel A) and lower image noise (Panel B) as compared to HIR and FBP. FBP: Filtered back projection; HIR: Hybrid iterative reconstruction; IMR: Iterative model reconstruction.

On quantitative image quality analysis median CT number in the aorta did not differ between the three reconstructions (492.3 [442.7–556.8] for FBP, 492.8 [443.0–556.8] for HIR and 491.3 [442.7–555.0] for IMR, $p = 1.00$). Higher luminal CT numbers ($p < 0.01$ all) were revealed in every assessed proximal and distal coronary artery segments with the use of IMR as compared to the other two reconstructions. No difference was observed between HIR and FBP for the respective coronary segment in HU values. Median attenuation values were similar or lower in the distal coronary segments using FBP and HIR reconstruction, as compared to the proximal coronary parts of the same vessel (LAD: $p = 0.71$ and $p = 0.69$; CX: $p < 0.01$ both, RCA: $p = 0.66$ and $p = 0.69$, respectively). Interestingly, IMR showed preserved or increased luminal contrast in the distal coronary segments as compared to the respective proximal coronary regions (LAD: $p < 0.01$; CX: $p = 0.18$; RCA: $p = 0.03$). **Table 4 and 5** indicates the changes in CT attenuation values and CNR for main coronary arteries across different reconstruction algorithms.

Table 4. Comparison of CT attenuation values between the proximal and distal coronary segments (88).

Data are presented as medians and interquartile ranges. CT attenuation is presented in Hounsfield units (HU). Difference between proximal and distal coronary segments was assessed using Wilcoxon signed ranks tests. Utilization of IMR has led to substantially higher CT attenuation values in the distal coronaries.

FBP: filtered back projection reconstruction; HIR: hybrid iterative reconstruction; IMR: iterative model reconstruction; LAD: left anterior descending coronary artery; CX: circumflex coronary artery; RCA: right coronary artery.

	LAD			CX			RCA		
	Proximal	*Distal*	*p value*	*Proximal*	*Distal*	*p value*	*Proximal*	*Distal*	*p value*
HU_{FBP}	509.6 [445.2-599.4]	492.3 [445.3-564.3]	0.071	506.5 [445.8-598.5]	447.0 [369.5-539.0]	<0.001	523.0 [441.0-601.8]	523.5 [445.8-581.8]	0.655
HU_{HIR}	510.6 [446.3-598.5]	487.9 [442.8-565.8]	0.069	510.5 [444.4-596.1]	434.5 [355.0-538.3]	<0.001	520.9 [441.9-603.0]	524.5 [449.5-581.0]	0.692
HU_{IMR}	534.5 [465.4-633.6]	572.6 [520.3-670.7]	0.001	563.3 [489.6-628.0]	537.6 [474.4-610.1]	0.177	546.5 [471.6-652.0]	561.9 [500.5-636.3]	0.026

DOI:10.14753/SE.2017.2079

Table 5. Comparison of CNR values between the proximal and distal coronary segments (88).

Data are presented as medians and interquartile ranges. Difference between proximal and distal coronary segments was assessed using Wilcoxon signed ranks tests. Utilization of IMR significantly improved CNR values as compared to FBP and HIR.

CNR: contrast-to-noise ratio; FBP: filtered back projection reconstruction; HIR: hybrid iterative reconstruction; IMR: iterative model reconstruction; LAD: left anterior descending coronary artery; CX: circumflex coronary artery; RCA: right coronary artery.

	LAD			CX			RCA		
	Proximal	*Distal*	*p value*	*Proximal*	*Distal*	*p value*	*Proximal*	*Distal*	*p value*
CNR_{FBP}	15.1 [11.7-18.0]	14.2 [11.6-17.7]	0.150	14.5 [11.8-18.0]	12.5 [9.7-16.1]	<0.001	14.6 [11.6-19.1]	14.3 [11.4-18.5]	0.616
CNR_{HIR}	21.5 [17.2-26.3]	20.7 [16.6-25.2]	0.145	20.8 [17.3-26.9]	18.3 [13.5-23.5]	<0.001	21.0 [16.8-27.8]	21.1 [16.9-26.5]	0.372
CNR_{IMR}	50.7 [45.2-59.0]	55.1 [45.4-63.6]	0.001	50.6 [45.3-58.4]	51.2 [38.9-55.5]	0.018	51.2 [43.1-61.3]	53.2 [46.6-62.9]	0.001

DOI:10.14753/SE.2017.2079

Image noise (SD) in the aorta was significantly different for FBP, HIR and IMR (42.6 [33.2-48.3], 29.4 [23.0-33.1] and 12.4 [11.0-13.8], respectively, $p < 0.01$ all). Noise reduction achieved by HIR and IMR was 31.5% and 66.9% as compared to FBP, respectively. HIR improved CNR in all assessed coronary segments, as compared to FBP, which was further improved with IMR ($p < 0.01$, both) **(Figure 18)**. Similarly, we detected significantly increased SNR values using IMR as compared to FBP or HIR ($p < 0.01$, both). Inter-observer agreement between quantitative parameters (CNR) was excellent with FBP, HIR and IMR reconstructions (correlation concordance coefficient: 0.97, 0.98 and 0.98, respectively).

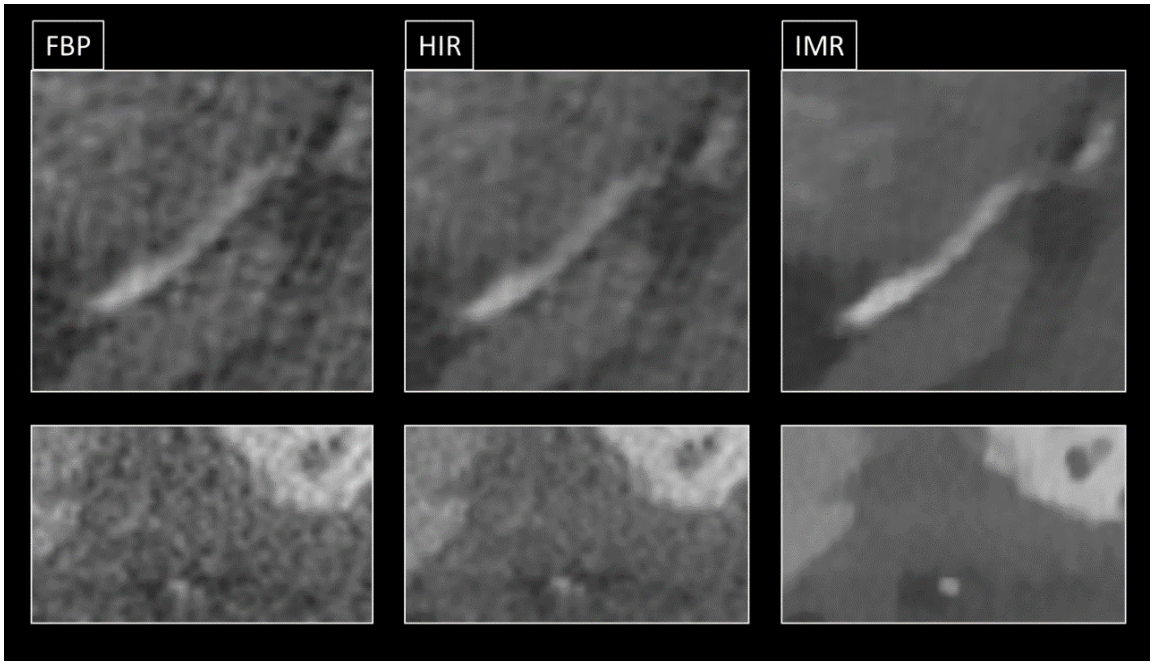

Figure 17. Representative case demonstrating improved distal coronary visualization using novel IMR algorithm as compared to FBP and HIR *(own material).*

DOI:10.14753/SE.2017.2079

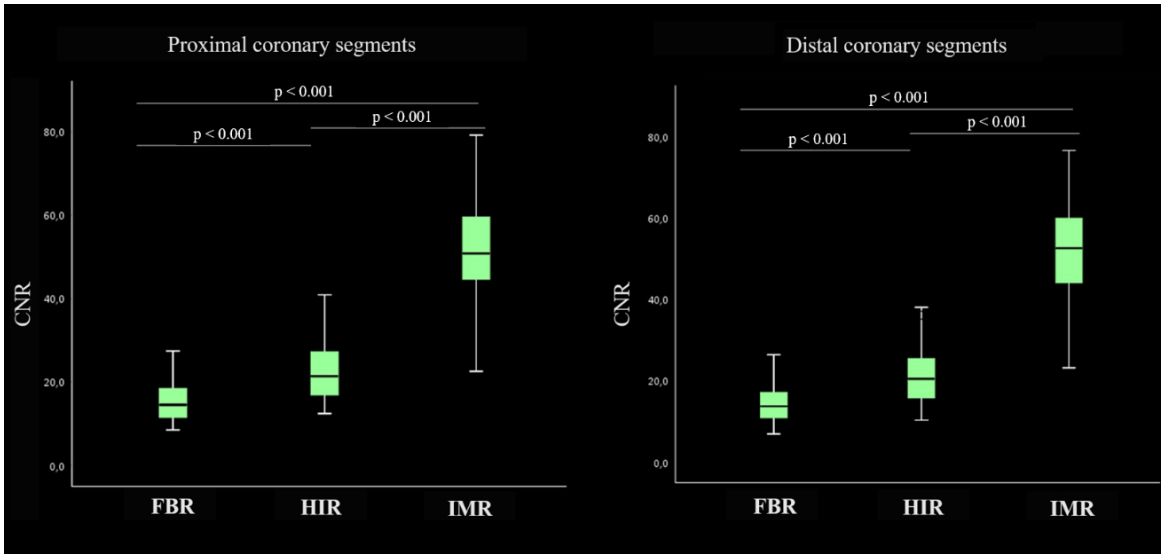

Figure 18. CNR values for the proximal and distal coronary segments for LAD, LCX and RCA *(own material).* We detected significant improvement using novel model based IR as compared to FBP or HIR ($p<0.001$ for all). The improved CNR values using IMR allows for better visualization of the coronaries and adjacent structures.

DOI:10.14753/SE.2017.2079

4.3 Model based iterative reconstruction reduces calcified plaque volume

The impact of novel IR algorithms was assessed on the same patient population as described in chapter 4.2. The results of the comprehensive plaque analysis are shown in **Table 6**.

The lesion length was 24.8 [16.0–28.8] mm and no significant difference was found among the three reconstructions. Overall plaque volume was lower with HIR as compared to FBP ($p = 0.02$), and further reduced by IMR ($p < 0.01$ all). Calcified plaque volume was highest with FBP and lowest with IMR (FBP vs. HIR $p = 0.006$; HIR vs. IMR $p = 0.017$; and FBP vs. IMR $p < 0.001$). High attenuation non-calcified plaque volumes with an attenuation ranging 90–129 HU yielded similar values with FBP and HIR ($p = 0.81$), however it was lower with IMR (HIR vs. IMR $p = 0.002$ and FBP vs. IMR $p < 0.001$). No difference was found between FBP, HIR and IMR in intermediate and low attenuation non-calcified plaque components ($p = 0.22$ and 0.67, respectively). Lumen volumes did not differ between different reconstructions ($p = 0.23$). Overall plaque burden was lowest with IMR and highest with FBP (0.38 for IMR [0.32–0.44], 0.42 for HIR [0.37–0.47] and 0.44 for FBP [0.38–0.50], $p < 0.05$ all). Volumes of various plaque components are summarized in **Table 5**. We used a fully automated method for plaque quantification, therefore inter-observer variability was not tested further.

DOI:10.14753/SE.2017.2079

Table 6. Plaque volume analysis with fixed threshold settings (88).

Data are presented as medians with interquartile ranges. Plaque volume values are presented in mm^3. Significant difference for all comparison combinations between the three reconstructions was assessed.

Pairwise comparisons are represented between the three reconstructions as follows: *: $p<0.05$ FBP vs. IMR; †: $p<0.05$ HIR vs. IMR; ‡: $p<0.05$ FBP vs. HIR. FBP: filtered back projection reconstruction; HIR: hybrid iterative reconstruction; IMR: iterative model reconstruction; HU: Hounsfield unit

				Non-calcified plaque volume			Calcified plaque volume
	Vessel Volume *†	Lumen Volume	Overall Plaque Volume *†‡	<30 HU	30-89 HU	90-129 HU *†	>130 HU *†‡
FBP	334.1 [228.1-477.9]	186.0 [126.0-264.5]	147.0 [100.7-183.6]	1.5 [0.3-4.3]	8.2 [2.8-15.3]	10.2 [5.2-20.3]	115.9 [81.7-164.2]
HIR	327.6 [227.6-473.9]	186.6 [129.5-271.6]	138.7 [90.6-191.7]	1.4 [0.4-3.7]	7.7 [3.0-13.2]	9.7 [5.4-18.7]	110.2 [63.8-166.6]
IMR	308.0 [202.7-466.8]	190.9 [102.8-266.3]	121.7 [79.3-168.4]	1.1 [0.3-2.8]	6.0 [3.2-10.3]	7.2 [4.6-16.2]	105.9 [62.1-144.6]

DOI:10.14753/SE.2017.2079

5. DISCUSSION

5.1 The use of iterative reconstruction for CAC assessment

In our study we have demonstrated that both hybrid-type and model based IR algorithms decrease the quantity of measured coronary artery calcium in comparison to the most widely used FBP algorithm. Moreover, we demonstrated an improved inter-reader reproducibility using IMR and HIR as compared to FBP algorithm. Finally, we have showed that IR techniques have a modest effect on cardiovascular risk stratification based on CAC scoring.

The utilization of novel IR techniques resulted in significantly lower CAC score in our study. The largest difference was found between FBP and IMR with relative difference of 7.3 %, while no significant difference was detected using HIR or IMR based on post hoc analysis. Previous studies showed significant reduction in image noise by using IMR with simultaneous dose reduction. In our study population HIR and IMR reduced noise by 33.9 and 65.8 % as compared to FBP, respectively. HIR and IMR resulted in reduced CAC values in comparison to FBP, but no difference was observed between HIR and IMR. The differences in calcium scores using HIR or IMR versus FBP might be due to the reduced noise and decreased blooming artefacts achieved by HIR and IMR techniques. However, phantom studies are needed for precise calcium volume quantification to validate the differences in CAC scoring between reconstruction algorithms.

The safety and feasibility of IR in CAC measurements was evaluated by prior studies using hybrid-type reconstruction method. Kurata et al. reported that with sinogram-affirmed IR algorithm calcium was no longer detected in some cases in comparison to FBP images (121). The disappearance of CAC values using IR as compared to FBP raised concerns that hybrid-type IR could eventually alter CAC based risk estimation. The reduction in CAC scores poses the risk of underestimating risk for clinical events. Under the disappearance of calcified plaque the authors meant, that using FBP the patient had minimal calcification, whereas using IR technique calcification was not assessable any more in the same patient. A recent study revealed that hybrid IR increased the number of patients with a calcium score of zero by 13 % (54). A significant decrease in CAC score

was described by using HIR as compared to FBP, and authors found that 29 % of the study population were moved to a lower risk category using HIR. These results are in line with our findings, however the reclassification rates were lower in our study. Importantly, we did not experience the disappearance of calcium in the coronary tree; the number of patients with zero CAC scores was not increased with the utilization of IMR. Gebhard et al. also evaluated the influence of hybrid-type IR of calcium scoring in 50 consecutive patients. In their study hybrid-type IR resulted in significantly lower Agatston scores as compared to FBP, and subsequently lead to an 18 % shift of patients to lower risk categories. Contrary to these previous observations in our study IMR and HIR lead to substantially lower reclassification rates as compared to FBP (122).

Our results and previous observations of other working groups highlight that substantial differences might exist between different reconstruction techniques provided by different vendors. Therefore, interplatform standardization is needed and reconstruction based adjustment of CAC values may be necessary in the future. Recently, Tatsugami et al. assessed the impact of latest generation HIR on radiation dose in CAC scoring and demonstrated that substantial radiation dose reduction can be achieved without altering CAC measurements (123). In our study we used the data of a cardiovascular screening program to estimate the risk reclassification rate due to IR methods in intermediate risk patients, and found that 2.4 % of individuals were reclassified using IMR. Although the study population had higher reclassification rate as compared to the test population, this can be explained by the higher CAC values of the symptomatic patient cohort. We found that IMR reduces the CAC values, however it has a moderate effect on the actual risk classification. Larger prospective studies are warranted to confirm our findings regarding the risk reclassification rates of asymptomatic population. Interestingly, Willemink et al. found substantially different CAC scores with using the state-of the-art CT scanners from four major vendors in an ex vivo study. The study simulated the reclassification rate on 432 participants at intermediate risk from the Rotterdam Study, and these differences resulted in risk reclassification of individuals in up to 6.5 % of cases, showing that CAC scores depends not only on patient characteristics and image reconstruction techniques but also on different scanner types (56).

Calcium scoring based atherosclerosis screening is widely utilized among asymptomatic individuals with intermediate cardiovascular risk, therefore we should consider to utilize the latest reconstruction techniques in order to lower radiation dose, however we should also keep in mind the potential influence of various reconstruction techniques on calcium quantification (124). This might be especially important in patient groups with higher CAC values (such as diabetes mellitus, hypertension or peripheral arterial disease) (125). High reproducibility of CAC scoring measurements is of utmost importance for cardiovascular screening and therapy monitoring. Reproducibility in CAC measurements was almost perfect using IMR and HIR. The lower inter- and intra-observer variability of IMR as compared to FBP shows its power and efficacy to identify coronary calcium without falsely delineating other areas with increased noise as calcification. Furthermore, the low variability of the measurements supports the use of IMR and HIR in CAC score assessment for patient follow-up.

Based on our findings we strongly encourage the use of correction factors when assessing patient's risk based on coronary calcium measures in the future. Prospective trials are warranted to validate such correction factors for reconstruction algorithms or scanner types. It is expected that IR algorithms will replace FBP images for image analysis as they provide lower doses. However, CAC measurements were established and validated using FBP images and thus further studies using IR are not necessarily comparable to prior ones.

DOI:10.14753/SE.2017.2079

5.2 Iterative reconstruction for improving image quality

We demonstrated that IMR improves both qualitative and quantitative coronary CTA image quality parameters over HIR and FBP. We found IMR to improve CNR in the proximal, as well in the distal coronary artery segments. Only a few studies evaluated the image quality of IMR for the evaluation of the coronary arteries in a clinical setting up until today (38,112,115,126). By using analogous scoring systems for overall image quality and image noise, previous studies also reported improved qualitative image quality parameters for cardiac CT (111,112). Quantitative analysis confirmed our subjective findings, as we revealed a substantial decrease in image noise using IMR as compared to HIR and FBP. The overall noise reduction of 66.9% with IMR and 31.5% with HIR in our study is comparable with the results of other research groups, which reported a noise reduction of 56.0–78.3% for IMR and 34.1–55.5% for HIR (112,115). Similarly, we observed increased CNR values in every assessed coronary segment with HIR as compared with FBP, which further improved with IMR. This finding is in line with other recent studies evaluating the performance of IMR in the cardiac setting. Interestingly, while median CT numbers were preserved in the aorta independent of applied image reconstruction technique, HU values in vessels with smaller caliber – proximal and distal segments of the coronary arteries – were higher with IMR as compared to the other two reconstructions. The median CT numbers did not differ between HIR and FBP in the respective coronary segments. Comparing the median values of attenuation in the distal coronary segments to the proximal ones of the same vessel, we found preserved or even increased median attenuation values using IMR. However, with HIR and FBP technique, the HU values were similar, or rather decreased from proximal to the distal coronary segments. Notably, a tendency for better visualization of the distal coronary segments was already described by Oda et al., though no difference was found in CT numbers among the three reconstructions between the proximal and distal coronary parts (40). In the study of Yuki et al. a clear drop of CT number was observed from proximal to distal, independent of image reconstruction (112). However, prior studies used lower tube voltage settings that might have influenced the distribution of HU values. In an ex vivo model using model based IR, Scheffel et al. also found higher median luminal CT numbers in the coronaries, as compared to HIR and standard FBP, while

difference between HIR and FBP was not observed either (118). Our findings for the median attenuation in the proximal, and distal segments of the coronary arteries are more in line with the study of Scheffel et al. and differ from those of Oda et al. Smaller structures are typically more affected by the partial volume effect. More ideal point spread function, greater edge-enhancement kernels and subsequently improved CNR ratio allowed by IMR might support the imaging of small structures (e.g. coronary branches), which are not always evaluable with noisier image reconstructions. The utilization of IMR could influence the median HU values in ROIs drawn close to the edge of small structures, since these ROIs are likely to be influenced by the point spread function effect on the edge. On the other hand, ROIs drawn in the middle of larger structures such as aorta are not close to the edges and hence are not affected and provide the median HU values that are comparable to FBP and HIR techniques. In clinical routine, standard reading of coronary stenosis is highly dependent on image quality and image noise. The use of IMR allows an excellent image quality by decreasing „graininess" of the CTA images, and also improves distal vessel visualization. As images remain of high diagnostic quality using IMR, significant dose reduction may be achieved, as reported by other studies.

DOI:10.14753/SE.2017.2079

5.3 Impact of the reconstruction method on plaque analysis

Coronary plaque quantification is in the focus of current cardiovascular imaging. Quantified plaque volumes and plaque composition might have prognostic utility and are also associated with myocardial ischemia. By quantitative coronary plaque assessment, we found a significant reduction in overall plaque volume and calcified plaque volume with the use of IMR as compared to HIR and FBP techniques. Interestingly, the image reconstruction technique did not influence non-calcified plaque volume, except for high-attenuation volume ranging 90–129 HU, which was reduced with IMR, but no difference was found between HIR and FBP. These findings contribute to the reduced overall plaque volumes measured with IMR. Low and intermediate attenuation non-calcified plaque volumes were not altered by the type of image reconstruction in our study. As the prognostic value of plaque volume for MACE beyond clinical risk scores has already been shown, alterations in plaque volume quantification could possibly reclassify patients and change prognostic information (127).

Although currently qualitative analysis is used for clinical decision making in coronary CTA, semi-automated plaque assessment is desirable for monitoring of long term plaque burden changes in individual patients. Only a few prior studies have assessed the effect of recently introduced IR techniques for this purpose. We used a software tool validated against intravascular ultrasound for fully automated volumetric plaque assessment (128). Contrary to our findings, two recently published studies demonstrated that HIR did not affect volumetric plaques assessment, while improved image quality as compared to FBP (100,101). Although, in the detailed analysis by Fuchs et al., who analyzed the plaque volume components in different HU strata, a significant decrease in calcified plaque components was reported with CT numbers between 401 and 500 HU. Moreover, a recent study by Puchner et al. reported the improved feasibility of automated plaque assessment with model-based IR, while it reduced the vessel-wall delineation incongruences, especially at the site of calcified plaques (102). This supports our hypothesis, that the decreased plaque volumes measured with IMR results mainly from the improved delineation of the calcified coronary atherosclerotic plaques.

DOI:10.14753/SE.2017.2079

5.4 Limitations

There are some limitations regarding the listed studies that have to be acknowledged. During the past decade all vendors have introduced hybrid and model type IR techniques to improve image quality. All of our results are derived from two different Philips IR algorithms (HIR and IMR, Philips, Best, The Netherlands), therefore it might not apply for all other vendor's iterative reconstruction. Another limitation is that we only measured CAC values and plaque volumes using medium noise reduction levels of iterative reconstructions, that is also applied in clinical settings. Different levels of iterative reconstructions might slightly influence our findings. We have evaluated the effects of IR on coronary calcification in a relatively small number of patients. Further investigation with larger patient number and different risk characteristics is needed for the analysis of CAC based risk reclassification. The higher radiation dose in the test population was the result of the higher tube current setting used in the test versus the study population (80 vs 30 mAs). The calcium scoring scans in the test population were acquired in the framework of an epidemiologic investigation with predefined scan parameters, whereas the study population scans were acquired as part of the routine clinical practice.

Regarding the scoring system used for subjective image quality analysis it might show individual differences by readers and the different visual appearance of reconstruction types (e.g. "blotchy" or plastic appearance of IMR images) does not enable truly blinded analysis. However, the good-to-excellent inter-observer reproducibility of the qualitative scoring supports the reliability of our data. Moreover, we demonstrated an excellent inter-reader reproducibility of quantitative image quality analysis. The applied plaque quantification method might be also considered as a limitation of our study. The manual setting of plaque start- and endpoints might introduce some errors in plaque volume measurements, however excessive care was taken to ensure that exactly the same lesion was measured by the different reconstruction techniques with identical lesion length. Accordingly, manual correction might be necessary in datasets of patients with higher HRs during data acquisition and this might introduce observer related differences in plaque volume quantification. There might also be an overlap between plaque components and our findings need to be validated against reference standard (e.g. intravascular ultrasound).

DOI:10.14753/SE.2017.2079

5.5 Future perspectives

Coronary CT angiography has emerged as a highly reliable and non-invasive modality for the exclusion of coronary artery disease. Due to recent advancements, CTA has the ability to assess the anatomy and functional relevance of a given lesion. State-of-the-art CT imaging applies IR algorithms to reduce radiation exposure related to coronary CTA. Notably, coronary artery calcium scoring remains a simple and robust tool for the assessment of cardiovascular risk.

Calcification is a hallmark feature of coronary atherosclerosis. CTA provides reliable information on calcification and the amount and distribution of coronary plaques. Coronary calcification and plaque involvement both reflect total coronary plaque burden, which is considered as a strong predictor of adverse cardiac events. Recent studies have demonstrated controversial results regarding the impact of novel IR techniques on coronary artery calcium scoring. The widespread use of IR for the reduction of image noise could significantly alter our risk assessment, as it led to the disappearance of calcified plaques in prior studies. Novel image reconstruction techniques should be carefully implemented in the clinical setting when assessing patients' risk using CAC or plaque volumes. We have shown a significant reduction in CAC scores using novel IR algorithms as compared to FBP. We encourage the use of correction factors for various types and levels of IR that might provide useful in the near future.

Growing body of evidence suggests that the density of calcification is associated with plaque stability, however evidence is still limited. Recently, the Multi-Ethnic Study of Atherosclerosis (MESA) has found that while increased CAC is associated with CAD and cardiac vascular disease, increased density was inversely related to CAD and CVD risk at any level of CAC volume (53). Studies evaluating the impact of statin therapy on plaque density are warranted in the future. Similarly, we currently have very limited data regarding contrast enhanced CTA based plaque assessment. It has been suggested that quantified plaque volume could provide important prognostic information for adverse events. Distinct plaque components are shown to be associated with myocardial ischemia (129). We have evaluated the impact of IR techniques on quantified plaque volume and composition. Based on our results, coronary calcium score and quantified calcified plaque volume were both reduced by IR techniques as compared to FBP. Consequently, we have

to carefully select the optimal IR technique for plaque assessment. Further studies are needed to evaluate the impact of different model based iterative reconstruction algorithms on risk stratification.

In recent years, robust noise reduction provided by IR allowed for the optimization of radiation dose. Dose saving algorithms in combination with IR enabled submillisievert image acquisition for coronary CTA. Excellent image quality is a prerequisite for proper plaque assessment and diagnosis. Recently several investigations have evaluated the image quality improvement due to IR methods. We performed a comprehensive image quality analysis of the coronary tree and found improved distal vessel visualization. Further studies should therefore focus on individual dose saving algorithms without reducing measured CAC or plaque volumes and establish the optimal level of IR for all vendors. Importantly, excellent image quality is also necessary for non-invasive fractional flow reserve assessment, that can provide reliable information on the hemodynamic significance of a given coronary lesion. Thus, we expect that FBP images will be mostly replaced by novel IR techniques in the near future for cardiac and other applications. Standardization of protocols across CT providers for plaque assessment is therefore desired.

DOI:10.14753/SE.2017.2079

6. CONCLUSIONS

In our study we found that IMR and HIR algorithms have led to substantial reduction in CAC scores. Changes in CAC score were associated with a modest reclassification rate in the study population. When translating the results to a larger test population, IR yielded a moderate reclassification rate of 2.4 % of 504 asymptomatic patients of a cardiovascular screening program. We did not detect the disappearance of calcium using IR algorithms. Also, we found excellent reproducibility of CAC using IR algorithms. The improved reproducibility of IR based CAC scoring could provide a more accurate risk prediction as compared to the noisier FBP images.

We demonstrated that the utilization of novel IR algorithms has led to significantly improved qualitative and quantitative coronary CTA image quality with improved visualization of the distal vessel segments as compared to traditional FBP. The number of non-diagnostic coronary segments were significantly lower using the most advanced model based IR technique as compared to traditional FBP. The use of novel IR algorithms is therefore strongly encouraged in clinical practice.

Furthermore, using automated plaque assessment we found that the use of IMR reduced both total and calcified plaque volume. Further studies are needed to evaluate the effects of these changes on individual risk prediction.

DOI:10.14753/SE.2017.2079

7. SUMMARY

Coronary CTA has emerged as a useful noninvasive tool for the detection of CAD. Novel image reconstruction algorithms hold the potential to significantly improve the image quality of CTA. Model based IR algorithm represents the latest advancement among IR techniques in clinical practice. We showed that model based and hybrid-type IR algorithms significantly improve both qualitative and quantitative image quality for the assessment of coronary arteries. The use of IMR has led to increased CNR and SNR values in both proximal and distal coronaries as compared to FBP. As a result of robust noise reduction the number of diagnostic segments were also significantly higher for IMR on visual assessment.

Coronary artery calcium scoring is a simple and effective method for the assessment the calcified plaque burden. In our study, we defined the optimal level of reconstruction for CT based calcium scoring. The use of IR was associated with reduced CAC scores as compared to FBP. However, subsequent changes in CAC based risk categories demonstrated only a modest reclassification rate in both the study and test populations, latter derived from a larger symptomatic patient cohort. Furthermore, we found that novel hybrid-type and model based IR techniques did not lead to the disappearance of small calcification on CT images as described by prior studies. Our results emphasize the use of novel IR algorithms to improve image quality, and its effect on calcified plaque burden quantification. On automated plaque assessment we found that IR also influences CTA based plaque quantification and characterization. We have shown that IMR decreased total and calcified plaque volumes. Moreover, our results have shown an improved reproducibility for CAC scoring and image quality assessment using IR algorithms as compared to traditional FBP reconstruction.

DOI:10.14753/SE.2017.2079

8. ÖSSZEFOGLALÁS

A koronária komputer tomográfia angiográfia (CTA) a koszorúér-betegség kimutatásának hatékony non-invazív képalkotó eszköze. Az elmúlt évek fejlesztései a képrekonstrukció terén a CTA képminőségének jelentős javulásához vezettek. Az iteratív képrekonstrukciós algoritmusok legújabb fejlesztését a model alapú iteratív képrekonstrukciós algoritmus jelenti. Vizsgálatunkban a model alapú és hybrid-típusú iteratív rekonstrukciós technikák alkalmazásával a kvalitatív és kvantitatív képminőség szignifikáns javulását tapasztaltuk a koronáriák elemzése során. A modell alapú képrekonstrukció a hagyományos szűrt-visszavetítéses rekonstrukcióval (FBP) összehasonlítva a kontraszt-zaj és jel-zaj arányok szignifikáns növekedéséhez vezetett. A nagymértékű zajcsökkentés következtében szignifikánsan magasabb volt a diagnosztikus szegmentumok aránya a képminőség szubjektív értékelése során.

A natív felvételeken mért koronária kálcium score egy egyszerű és jól reprodukálható módszer a kalcifikált plakkok meghatározására. Vizsgálatunkban meghatároztuk az optimális iteratív rekonstrukciós szintet a CT alapú kálcium score kiszámítására. Az iteratív képrekonstrukció alkalmazása jelentősen alacsonyabb kálcium pontértéket eredményezett FBP-hez képest. A kálcium pontérték alapján meghatározott rizikócsoportokban ez a különbség azonban csak kis mértékű reklasszifikációt eredményezett mind a vizsgálati mind a teszt populációban, mely utóbbi egy nagyobb epidemiológiai vizsgálat betegeit tartalmazta. Korábbi vizsgálatokkal ellentétben az új iteratív képrekonstrukció alkalmazása nem vezetett a kalcifikált plakkok eltűnéséhez. Eredményeink alapján az iteratív rekonstrukciós algoritmus kiemelten fontos a képminőség javításának érdekében. Ezen felül eredményeink rávilágítanak a képrekonstrukciós algoritmusok kalcifikált plakkokra gyakorolt hatásaira is. Automatikus plakk elemzés révén vizsgálatunkban megállapítottuk, hogy az új típusú iteratív rekonstrukciós technikák a plakkok kvantifikációját és karakterizációját is befolyásolhatja. Nevezetesen, jelentősen alacsonyabb kalcifikált és teljes plakktérfogatot mértünk a model alapú algoritmus alkalmazásával FBP-vel szemben. Továbbá vizsgálatunkban az új rekonstrukciós technika magasabb reprodukálhatóságát igazoltuk a képminőség és a kálcium pontérték elemzése során, ami kiemelten fontos a megbízható képelemzéshez és betegeink rizikójának becslése során.

9. BIBLIOGRAPHY

1. Mensah GA, Moran AE, Roth GA, Narula J. (2014) The global burden of cardiovascular diseases, 1990-2010. Glob Heart, 9: 183-184.
2. Fuster V. (2014) Global burden of cardiovascular disease: time to implement feasible strategies and to monitor results. J Am Coll Cardiol, 64: 520-522.
3. Writing Group M, Mozaffarian D, Benjamin EJ, Go AS, Arnett DK, Blaha MJ, Cushman M, Das SR, de Ferranti S, Despres JP, Fullerton HJ, Howard VJ, Huffman MD, Isasi CR, Jimenez MC, Judd SE, Kissela BM, Lichtman JH, Lisabeth LD, Liu S, Mackey RH, Magid DJ, McGuire DK, Mohler ER, 3rd, Moy CS, Muntner P, Mussolino ME, Nasir K, Neumar RW, Nichol G, Palaniappan L, Pandey DK, Reeves MJ, Rodriguez CJ, Rosamond W, Sorlie PD, Stein J, Towfighi A, Turan TN, Virani SS, Woo D, Yeh RW, Turner MB, American Heart Association Statistics C, Stroke Statistics S. (2016) Heart Disease and Stroke Statistics-2016 Update: A Report From the American Heart Association. Circulation, 133: e38-360.
4. Nichols M, Townsend N, Scarborough P, Rayner M. (2014) Cardiovascular disease in Europe 2014: epidemiological update. Eur Heart J, 35: 2929.
5. Hulten E, Bittencourt MS, Singh A, O'Leary D, Christman MP, Osmani W, Abbara S, Steigner ML, Truong QA, Nasir K, Rybicki FF, Klein J, Hainer J, Brady TJ, Hoffmann U, Ghoshhajra BB, Hachamovitch R, Di Carli MF, Blankstein R. (2014) Coronary artery disease detected by coronary computed tomographic angiography is associated with intensification of preventive medical therapy and lower low-density lipoprotein cholesterol. Circ Cardiovasc Imaging, 7: 629-638.
6. Westerby R. (2011) An overview of cardiovascular disease risk assessment. Nurs Stand, 26: 48-55; quiz 56.
7. Trogdon JG, Finkelstein EA, Nwaise IA, Tangka FK, Orenstein D. (2007) The economic burden of chronic cardiovascular disease for major insurers. Health Promot Pract, 8: 234-242.
8. Task Force M, Montalescot G, Sechtem U, Achenbach S, Andreotti F, Arden C, Budaj A, Bugiardini R, Crea F, Cuisset T, Di Mario C, Ferreira JR, Gersh BJ, Gitt AK, Hulot JS, Marx N, Opie LH, Pfisterer M, Prescott E, Ruschitzka F, Sabate M, Senior R, Taggart DP, van der Wall EE, Vrints CJ, Guidelines ESCCfP, Zamorano JL,

Achenbach S, Baumgartner H, Bax JJ, Bueno H, Dean V, Deaton C, Erol C, Fagard R, Ferrari R, Hasdai D, Hoes AW, Kirchhof P, Knuuti J, Kolh P, Lancellotti P, Linhart A, Nihoyannopoulos P, Piepoli MF, Ponikowski P, Sirnes PA, Tamargo JL, Tendera M, Torbicki A, Wijns W, Windecker S, Document R, Knuuti J, Valgimigli M, Bueno H, Claeys MJ, Donner-Banzhoff N, Erol C, Frank H, Funck-Brentano C, Gaemperli O, Gonzalez-Juanatey JR, Hamilos M, Hasdai D, Husted S, James SK, Kervinen K, Kolh P, Kristensen SD, Lancellotti P, Maggioni AP, Piepoli MF, Pries AR, Romeo F, Ryden L, Simoons ML, Sirnes PA, Steg PG, Timmis A, Wijns W, Windecker S, Yildirir A, Zamorano JL. (2013) 2013 ESC guidelines on the management of stable coronary artery disease: the Task Force on the management of stable coronary artery disease of the European Society of Cardiology. Eur Heart J, 34: 2949-3003.

9. Budoff MJ, Jollis JG, Dowe D, Min J, Group VCTS. (2013) Diagnostic accuracy of coronary artery calcium for obstructive disease: results from the ACCURACY trial. Int J Cardiol, 166: 505-508.

10. Maffei E, Martini C, Tedeschi C, Spagnolo P, Zuccarelli A, Arcadi T, Guaricci A, Seitun S, Weustink A, Mollet N, Cademartiri F. (2011) Diagnostic accuracy of 64-slice computed tomography coronary angiography in a large population of patients without revascularisation: registry data on the impact of calcium score. Radiol Med, 116: 1000-1013.

11. Budoff MJ, Gopal A, Gopalakrishnan D. (2006) Cardiac computed tomography: diagnostic utility and integration in clinical practice. Clin Cardiol, 29: I4-14.

12. Hoffmann U, Ferencik M, Cury RC, Pena AJ. (2006) Coronary CT angiography. J Nucl Med, 47: 797-806.

13. Hoffmann U, Ferencik M, Udelson JE, Picard MH, Truong QA, Patel MR, Huang M, Pencina M, Mark DB, Heitner JF, Fordyce CB, Pellikka PA, Tardif JC, Budoff M, Nahhas G, Chow B, Kosinski AS, Lee KL, Douglas PS, Investigators P. (2017) Prognostic Value of Noninvasive Cardiovascular Testing in Patients With Stable Chest Pain: Insights From the PROMISE Trial (Prospective Multicenter Imaging Study for Evaluation of Chest Pain). Circulation, 135: 2320-2332.

14. Ladeiras-Lopes R, Bettencourt N, Ferreira N, Sampaio F, Pires-Morais G, Santos L, Melica B, Rodrigues A, Braga P, Leite-Moreira A, Silva-Cardoso J, Gama V.

(2016) CT myocardial perfusion and coronary CT angiography: Influence of coronary calcium on a stress-rest protocol. J Cardiovasc Comput Tomogr, 10: 215-220.

15. Leipsic J, Yang TH, Thompson A, Koo BK, Mancini GB, Taylor C, Budoff MJ, Park HB, Berman DS, Min JK. (2014) CT angiography (CTA) and diagnostic performance of noninvasive fractional flow reserve: results from the Determination of Fractional Flow Reserve by Anatomic CTA (DeFACTO) study. AJR Am J Roentgenol, 202: 989-994.

16. Cury RC, Abbara S, Achenbach S, Agatston A, Berman DS, Budoff MJ, Dill KE, Jacobs JE, Maroules CD, Rubin GD, Rybicki FJ, Schoepf UJ, Shaw LJ, Stillman AE, White CS, Woodard PK, Leipsic JA. (2016) Coronary Artery Disease - Reporting and Data System (CAD-RADS): An Expert Consensus Document of SCCT, ACR and NASCI: Endorsed by the ACC. JACC Cardiovasc Imaging, 9: 1099-1113.

17. Detrano R, Guerci AD, Carr JJ, Bild DE, Burke G, Folsom AR, Liu K, Shea S, Szklo M, Bluemke DA, O'Leary DH, Tracy R, Watson K, Wong ND, Kronmal RA. (2008) Coronary calcium as a predictor of coronary events in four racial or ethnic groups. N Engl J Med, 358: 1336-1345.

18. Nasir K, Bittencourt MS, Blaha MJ, Blankstein R, Agatson AS, Rivera JJ, Miedema MD, Sibley CT, Shaw LJ, Blumenthal RS, Budoff MJ, Krumholz HM. (2015) Implications of Coronary Artery Calcium Testing Among Statin Candidates According to American College of Cardiology/American Heart Association Cholesterol Management Guidelines: MESA (Multi-Ethnic Study of Atherosclerosis). J Am Coll Cardiol, 66: 1657-1668.

19. Agatston AS, Janowitz WR, Hildner FJ, Zusmer NR, Viamonte M, Jr., Detrano R. (1990) Quantification of coronary artery calcium using ultrafast computed tomography. J Am Coll Cardiol, 15: 827-832.

20. Hou ZH, Lu B, Gao Y, Jiang SL, Wang Y, Li W, Budoff MJ. (2012) Prognostic value of coronary CT angiography and calcium score for major adverse cardiac events in outpatients. JACC Cardiovasc Imaging, 5: 990-999.

21. Budoff MJ, Shaw LJ, Liu ST, Weinstein SR, Mosler TP, Tseng PH, Flores FR, Callister TQ, Raggi P, Berman DS. (2007) Long-term prognosis associated with coronary calcification: observations from a registry of 25,253 patients. J Am Coll Cardiol, 49: 1860-1870.

22. Maurovich-Horvat P, Ferencik M, Voros S, Merkely B, Hoffmann U. (2014) Comprehensive plaque assessment by coronary CT angiography. Nat Rev Cardiol, 11: 390-402.
23. Abbara S, Blanke P, Maroules CD, Cheezum M, Choi AD, Han BK, Marwan M, Naoum C, Norgaard BL, Rubinshtein R, Schoenhagen P, Villines T, Leipsic J. (2016) SCCT guidelines for the performance and acquisition of coronary computed tomographic angiography: A report of the society of Cardiovascular Computed Tomography Guidelines Committee: Endorsed by the North American Society for Cardiovascular Imaging (NASCI). J Cardiovasc Comput Tomogr, 10: 435-449.
24. Wu FZ, Wu MT. (2015) 2014 SCCT guidelines for the interpretation and reporting of coronary CT angiography: a report of the Society of Cardiovascular Computed Tomography Guidelines Committee. J Cardiovasc Comput Tomogr, 9: e3.
25. Ferencik M, Mayrhofer T, Puchner SB, Lu MT, Maurovich-Horvat P, Liu T, Ghemigian K, Kitslaar P, Broersen A, Bamberg F, Truong QA, Schlett CL, Hoffmann U. (2015) Computed tomography-based high-risk coronary plaque score to predict acute coronary syndrome among patients with acute chest pain--Results from the ROMICAT II trial. J Cardiovasc Comput Tomogr, 9: 538-545.
26. Siegel JA, Welsh JS. (2016) Does Imaging Technology Cause Cancer? Debunking the Linear No-Threshold Model of Radiation Carcinogenesis. Technol Cancer Res Treat, 15: 249-256.
27. Westra SJ. (2014) The communication of the radiation risk from CT in relation to its clinical benefit in the era of personalized medicine: part 1: the radiation risk from CT. Pediatr Radiol, 44 Suppl 3: 515-518.
28. Zhu X, Zhu Y, Xu H, Yang G, Tang L, Xu Y. (2013) Dual-source CT coronary angiography involving injection protocol with iodine load tailored to patient body weight and body mass index: estimation of optimal contrast material dose. Acta Radiol, 54: 149-155.
29. Lell M, Marwan M, Schepis T, Pflederer T, Anders K, Flohr T, Allmendinger T, Kalender W, Ertel D, Thierfelder C, Kuettner A, Ropers D, Daniel WG, Achenbach S. (2009) Prospectively ECG-triggered high-pitch spiral acquisition for coronary CT angiography using dual source CT: technique and initial experience. Eur Radiol, 19: 2576-2583.

30. Maurovich-Horvat P, Karolyi M, Horvath T, Szilveszter B, Bartykowszki A, Jermendy AL, Panajotu A, Celeng C, Suhai FI, Major GP, Csobay-Novak C, Huttl K, Merkely B. (2015) Esmolol is noninferior to metoprolol in achieving a target heart rate of 65 beats/min in patients referred to coronary CT angiography: a randomized controlled clinical trial. J Cardiovasc Comput Tomogr, 9: 139-145.

31. Bischoff B, Hein F, Meyer T, Hadamitzky M, Martinoff S, Schomig A, Hausleiter J. (2009) Impact of a reduced tube voltage on CT angiography and radiation dose: results of the PROTECTION I study. JACC Cardiovasc Imaging, 2: 940-946.

32. Hausleiter J, Meyer T. (2008) Tips to minimize radiation exposure. J Cardiovasc Comput Tomogr, 2: 325-327.

33. Deseive S, Chen MY, Korosoglou G, Leipsic J, Martuscelli E, Carrascosa P, Mirsadraee S, White C, Hadamitzky M, Martinoff S, Menges AL, Bischoff B, Massberg S, Hausleiter J. (2015) Prospective Randomized Trial on Radiation Dose Estimates of CT Angiography Applying Iterative Image Reconstruction: The PROTECTION V Study. JACC Cardiovasc Imaging, 8: 888-896.

34. Hausleiter J, Meyer TS, Martuscelli E, Spagnolo P, Yamamoto H, Carrascosa P, Anger T, Lehmkuhl L, Alkadhi H, Martinoff S, Hadamitzky M, Hein F, Bischoff B, Kuse M, Schomig A, Achenbach S. (2012) Image quality and radiation exposure with prospectively ECG-triggered axial scanning for coronary CT angiography: the multicenter, multivendor, randomized PROTECTION-III study. JACC Cardiovasc Imaging, 5: 484-493.

35. Hausleiter J, Martinoff S, Hadamitzky M, Martuscelli E, Pschierer I, Feuchtner GM, Catalan-Sanz P, Czermak B, Meyer TS, Hein F, Bischoff B, Kuse M, Schomig A, Achenbach S. (2010) Image quality and radiation exposure with a low tube voltage protocol for coronary CT angiography results of the PROTECTION II Trial. JACC Cardiovasc Imaging, 3: 1113-1123.

36. Benz DC, Fuchs TA, Grani C, Studer Bruengger AA, Clerc OF, Mikulicic F, Messerli M, Stehli J, Possner M, Pazhenkottil AP, Gaemperli O, Kaufmann PA, Buechel RR. (2017) Head-to-head comparison of adaptive statistical and model-based iterative reconstruction algorithms for submillisievert coronary CT angiography. Eur Heart J Cardiovasc Imaging.

37. de Graaf FR, Schuijf JD, Delgado V, van Velzen JE, Kroft LJ, de Roos A, Jukema JW, van der Wall EE, Bax JJ. (2010) Clinical application of CT coronary angiography: state of the art. Heart Lung Circ, 19: 107-116.
38. Iyama Y, Nakaura T, Kidoh M, Oda S, Utsunomiya D, Sakaino N, Tokuyasu S, Osakabe H, Harada K, Yamashita Y. (2016) Submillisievert Radiation Dose Coronary CT Angiography: Clinical Impact of the Knowledge-Based Iterative Model Reconstruction. Acad Radiol, 23: 1393-1401.
39. den Harder AM, Wolterink JM, Willemink MJ, Schilham AM, de Jong PA, Budde RP, Nathoe HM, Isgum I, Leiner T. (2016) Submillisievert coronary calcium quantification using model-based iterative reconstruction: A within-patient analysis. Eur J Radiol, 85: 2152-2159.
40. Oda S, Weissman G, Vembar M, Weigold WG. (2014) Iterative model reconstruction: improved image quality of low-tube-voltage prospective ECG-gated coronary CT angiography images at 256-slice CT. Eur J Radiol, 83: 1408-1415.
41. Pletcher MJ, Sibley CT, Pignone M, Vittinghoff E, Greenland P. (2013) Interpretation of the coronary artery calcium score in combination with conventional cardiovascular risk factors: the Multi-Ethnic Study of Atherosclerosis (MESA). Circulation, 128: 1076-1084.
42. Pletcher MJ, Tice JA, Pignone M, Browner WS. (2004) Using the coronary artery calcium score to predict coronary heart disease events: a systematic review and meta-analysis. Arch Intern Med, 164: 1285-1292.
43. Shaw LJ, Raggi P, Schisterman E, Berman DS, Callister TQ. (2003) Prognostic value of cardiac risk factors and coronary artery calcium screening for all-cause mortality. Radiology, 228: 826-833.
44. Sarwar A, Shaw LJ, Shapiro MD, Blankstein R, Hoffmann U, Cury RC, Abbara S, Brady TJ, Budoff MJ, Blumenthal RS, Nasir K. (2009) Diagnostic and prognostic value of absence of coronary artery calcification. JACC Cardiovasc Imaging, 2: 675-688.
45. Kondos GT, Hoff JA, Sevrukov A, Daviglus ML, Garside DB, Devries SS, Chomka EV, Liu K. (2003) Electron-beam tomography coronary artery calcium and cardiac events: a 37-month follow-up of 5635 initially asymptomatic low- to intermediate-risk adults. Circulation, 107: 2571-2576.

46. Greenland P, LaBree L, Azen SP, Doherty TM, Detrano RC. (2004) Coronary artery calcium score combined with Framingham score for risk prediction in asymptomatic individuals. JAMA, 291: 210-215.
47. Tota-Maharaj R, Blaha MJ, McEvoy JW, Blumenthal RS, Muse ED, Budoff MJ, Shaw LJ, Berman DS, Rana JS, Rumberger J, Callister T, Rivera J, Agatston A, Nasir K. (2012) Coronary artery calcium for the prediction of mortality in young adults <45 years old and elderly adults >75 years old. Eur Heart J, 33: 2955-2962.
48. Raggi P, Shaw LJ, Berman DS, Callister TQ. (2004) Prognostic value of coronary artery calcium screening in subjects with and without diabetes. J Am Coll Cardiol, 43: 1663-1669.
49. Sung KC, Ryu S, Lee JY, Lee SH, Cheong ES, Wild SH, Byrne CD. (2016) Fatty Liver, Insulin Resistance, and Obesity: Relationships With Increase in Coronary Artery Calcium Over Time. Clin Cardiol, 39: 321-328.
50. Kwak MS, Yim JY, Kim D, Park MJ, Lim SH, Yang JI, Chung GE, Kim YS, Yang SY, Kim MN, Lee CH, Yoon JH, Lee HS. (2015) Nonalcoholic fatty liver disease is associated with coronary artery calcium score in diabetes patients with higher HbA1c. Diabetol Metab Syndr, 7: 28.
51. Nakanishi R, Rajani R, Cheng VY, Gransar H, Nakazato R, Shmilovich H, Otaki Y, Hayes SW, Thomson LE, Friedman JD, Slomka PJ, Berman DS, Dey D. (2011) Increase in epicardial fat volume is associated with greater coronary artery calcification progression in subjects at intermediate risk by coronary calcium score: a serial study using non-contrast cardiac CT. Atherosclerosis, 218: 363-368.
52. Puchner SB, Lu MT, Mayrhofer T, Liu T, Pursnani A, Ghoshhajra BB, Truong QA, Wiviott SD, Fleg JL, Hoffmann U, Ferencik M. (2015) High-risk coronary plaque at coronary CT angiography is associated with nonalcoholic fatty liver disease, independent of coronary plaque and stenosis burden: results from the ROMICAT II trial. Radiology, 274: 693-701.
53. Criqui MH, Denenberg JO, Ix JH, McClelland RL, Wassel CL, Rifkin DE, Carr JJ, Budoff MJ, Allison MA. (2014) Calcium density of coronary artery plaque and risk of incident cardiovascular events. JAMA, 311: 271-278.
54. van Osch JA, Mouden M, van Dalen JA, Timmer JR, Reiffers S, Knollema S, Greuter MJ, Ottervanger JP, Jager PL. (2014) Influence of iterative image

reconstruction on CT-based calcium score measurements. Int J Cardiovasc Imaging, 30: 961-967.

55. Funabashi N, Irie R, Namihira Y, Morimoto R, Aiba M, Ozawa K, Takaoka H, Ohta J, Masuda Y, Kobayashi Y. (2015) Influence of tube voltage and heart rate on the Agatston calcium score using an in vitro, novel ECG-gated dual energy reconstruction 320 slice CT technique. Int J Cardiol, 180: 218-220.

56. Willemink MJ, Vliegenthart R, Takx RA, Leiner T, Budde RP, Bleys RL, Das M, Wildberger JE, Prokop M, Buls N, de Mey J, Schilham AM, de Jong PA. (2014) Coronary artery calcification scoring with state-of-the-art CT scanners from different vendors has substantial effect on risk classification. Radiology, 273: 695-702.

57. Versteylen MO, Joosen IA, Shaw LJ, Narula J, Hofstra L. (2011) Comparison of Framingham, PROCAM, SCORE, and Diamond Forrester to predict coronary atherosclerosis and cardiovascular events. J Nucl Cardiol, 18: 904-911.

58. Arbab-Zadeh A, Fuster V. (2015) The myth of the "vulnerable plaque": transitioning from a focus on individual lesions to atherosclerotic disease burden for coronary artery disease risk assessment. J Am Coll Cardiol, 65: 846-855.

59. Otsuka K, Fukuda S, Tanaka A, Nakanishi K, Taguchi H, Yoshikawa J, Shimada K, Yoshiyama M. (2013) Napkin-ring sign on coronary CT angiography for the prediction of acute coronary syndrome. JACC Cardiovasc Imaging, 6: 448-457.

60. Willemink MJ, Leiner T, Maurovich-Horvat P. (2016) Cardiac CT Imaging of Plaque Vulnerability: Hype or Hope? Curr Cardiol Rep, 18: 37.

61. Mancini GB, Hartigan PM, Shaw LJ, Berman DS, Hayes SW, Bates ER, Maron DJ, Teo K, Sedlis SP, Chaitman BR, Weintraub WS, Spertus JA, Kostuk WJ, Dada M, Booth DC, Boden WE. (2014) Predicting outcome in the COURAGE trial (Clinical Outcomes Utilizing Revascularization and Aggressive Drug Evaluation): coronary anatomy versus ischemia. JACC Cardiovasc Interv, 7: 195-201.

62. Virmani R, Kolodgie FD, Burke AP, Farb A, Schwartz SM. (2000) Lessons from sudden coronary death: a comprehensive morphological classification scheme for atherosclerotic lesions. Arterioscler Thromb Vasc Biol, 20: 1262-1275.

63. Burke AP, Farb A, Malcom GT, Liang Y, Smialek JE, Virmani R. (1999) Plaque rupture and sudden death related to exertion in men with coronary artery disease. JAMA, 281: 921-926.

64. Arbustini E, Dal Bello B, Morbini P, Burke AP, Bocciarelli M, Specchia G, Virmani R. (1999) Plaque erosion is a major substrate for coronary thrombosis in acute myocardial infarction. Heart, 82: 269-272.

65. Virmani R, Burke AP, Kolodgie FD, Farb A. (2002) Vulnerable plaque: the pathology of unstable coronary lesions. J Interv Cardiol, 15: 439-446.

66. Nabel EG, Braunwald E. (2012) A tale of coronary artery disease and myocardial infarction. N Engl J Med, 366: 54-63.

67. Andreou I, Antoniadis AP, Shishido K, Papafaklis MI, Koskinas KC, Chatzizisis YS, Coskun AU, Edelman ER, Feldman CL, Stone PH. (2015) How do we prevent the vulnerable atherosclerotic plaque from rupturing? Insights from in vivo assessments of plaque, vascular remodeling, and local endothelial shear stress. J Cardiovasc Pharmacol Ther, 20: 261-275.

68. Osborn EA, Jaffer FA. (2013) Imaging atherosclerosis and risk of plaque rupture. Curr Atheroscler Rep, 15: 359.

69. Kolodgie FD, Burke AP, Farb A, Gold HK, Yuan J, Narula J, Finn AV, Virmani R. (2001) The thin-cap fibroatheroma: a type of vulnerable plaque: the major precursor lesion to acute coronary syndromes. Curr Opin Cardiol, 16: 285-292.

70. Finn AV, Nakano M, Narula J, Kolodgie FD, Virmani R. (2010) Concept of vulnerable/unstable plaque. Arterioscler Thromb Vasc Biol, 30: 1282-1292.

71. Virmani R, Burke AP, Farb A, Kolodgie FD. (2006) Pathology of the vulnerable plaque. J Am Coll Cardiol, 47: C13-18.

72. Motoyama S, Sarai M, Harigaya H, Anno H, Inoue K, Hara T, Naruse H, Ishii J, Hishida H, Wong ND, Virmani R, Kondo T, Ozaki Y, Narula J. (2009) Computed tomographic angiography characteristics of atherosclerotic plaques subsequently resulting in acute coronary syndrome. J Am Coll Cardiol, 54: 49-57.

73. Burke AP, Farb A, Malcom GT, Liang YH, Smialek J, Virmani R. (1997) Coronary risk factors and plaque morphology in men with coronary disease who died suddenly. N Engl J Med, 336: 1276-1282.

74. Narula J, Nakano M, Virmani R, Kolodgie FD, Petersen R, Newcomb R, Malik S, Fuster V, Finn AV. (2013) Histopathologic characteristics of atherosclerotic coronary disease and implications of the findings for the invasive and noninvasive detection of vulnerable plaques. J Am Coll Cardiol, 61: 1041-1051.

75. Pedrazzini GB, D'Angeli I, Vassalli G, Faletra FF, Klersy C, Pasotti E, Corbacelli C, Moccetti T, Auricchio A. (2011) Assessment of coronary stenosis, plaque burden and remodeling by multidetector computed tomography in patients referred for suspected coronary artery disease. J Cardiovasc Med (Hagerstown), 12: 122-130.
76. Motoyama S, Kondo T, Sarai M, Sugiura A, Harigaya H, Sato T, Inoue K, Okumura M, Ishii J, Anno H, Virmani R, Ozaki Y, Hishida H, Narula J. (2007) Multislice computed tomographic characteristics of coronary lesions in acute coronary syndromes. J Am Coll Cardiol, 50: 319-326.
77. Maurovich-Horvat P, Hoffmann U, Vorpahl M, Nakano M, Virmani R, Alkadhi H. (2010) The napkin-ring sign: CT signature of high-risk coronary plaques? JACC Cardiovasc Imaging, 3: 440-444.
78. Seifarth H, Schlett CL, Nakano M, Otsuka F, Karolyi M, Liew G, Maurovich-Horvat P, Alkadhi H, Virmani R, Hoffmann U. (2012) Histopathological correlates of the napkin-ring sign plaque in coronary CT angiography. Atherosclerosis, 224: 90-96.
79. Maurovich-Horvat P, Schlett CL, Alkadhi H, Nakano M, Otsuka F, Stolzmann P, Scheffel H, Ferencik M, Kriegel MF, Seifarth H, Virmani R, Hoffmann U. (2012) The napkin-ring sign indicates advanced atherosclerotic lesions in coronary CT angiography. JACC Cardiovasc Imaging, 5: 1243-1252.
80. Al-Mallah MH, Qureshi W, Lin FY, Achenbach S, Berman DS, Budoff MJ, Callister TQ, Chang HJ, Cademartiri F, Chinnaiyan K, Chow BJ, Cheng VY, Delago A, Gomez M, Hadamitzky M, Hausleiter J, Kaufmann PA, Leipsic J, Maffei E, Raff G, Shaw LJ, Villines TC, Cury RC, Feuchtner G, Plank F, Kim YJ, Dunning AM, Min JK. (2014) Does coronary CT angiography improve risk stratification over coronary calcium scoring in symptomatic patients with suspected coronary artery disease? Results from the prospective multicenter international CONFIRM registry. Eur Heart J Cardiovasc Imaging, 15: 267-274.
81. Min JK, Dunning A, Lin FY, Achenbach S, Al-Mallah M, Budoff MJ, Cademartiri F, Callister TQ, Chang HJ, Cheng V, Chinnaiyan K, Chow BJ, Delago A, Hadamitzky M, Hausleiter J, Kaufmann P, Maffei E, Raff G, Shaw LJ, Villines T, Berman DS, Investigators C. (2011) Age- and sex-related differences in all-cause mortality risk based on coronary computed tomography angiography findings results from the International Multicenter CONFIRM (Coronary CT Angiography Evaluation

for Clinical Outcomes: An International Multicenter Registry) of 23,854 patients without known coronary artery disease. J Am Coll Cardiol, 58: 849-860.

82. Lin FY, Shaw LJ, Dunning AM, Labounty TM, Choi JH, Weinsaft JW, Koduru S, Gomez MJ, Delago AJ, Callister TQ, Berman DS, Min JK. (2011) Mortality risk in symptomatic patients with nonobstructive coronary artery disease: a prospective 2-center study of 2,583 patients undergoing 64-detector row coronary computed tomographic angiography. J Am Coll Cardiol, 58: 510-519.

83. Bittencourt MS, Hulten E, Ghoshhajra B, O'Leary D, Christman MP, Montana P, Truong QA, Steigner M, Murthy VL, Rybicki FJ, Nasir K, Gowdak LH, Hainer J, Brady TJ, Di Carli MF, Hoffmann U, Abbara S, Blankstein R. (2014) Prognostic value of nonobstructive and obstructive coronary artery disease detected by coronary computed tomography angiography to identify cardiovascular events. Circ Cardiovasc Imaging, 7: 282-291.

84. Nakazato R, Arsanjani R, Achenbach S, Gransar H, Cheng VY, Dunning A, Lin FY, Al-Mallah M, Budoff MJ, Callister TQ, Chang HJ, Cademartiri F, Chinnaiyan K, Chow BJ, Delago A, Hadamitzky M, Hausleiter J, Kaufmann P, Raff G, Shaw LJ, Villines T, Cury RC, Feuchtner G, Kim YJ, Leipsic J, Berman DS, Min JK. (2014) Age-related risk of major adverse cardiac event risk and coronary artery disease extent and severity by coronary CT angiography: results from 15 187 patients from the International Multisite CONFIRM Study. Eur Heart J Cardiovasc Imaging, 15: 586-594.

85. de Araujo Goncalves P, Garcia-Garcia HM, Dores H, Carvalho MS, Jeronimo Sousa P, Marques H, Ferreira A, Cardim N, Campante Teles R, Raposo L, Mesquita Gabriel H, Sousa Almeida M, Aleixo A, Mota Carmo M, Pereira Machado F, Mendes M. (2013) Coronary computed tomography angiography-adapted Leaman score as a tool to noninvasively quantify total coronary atherosclerotic burden. Int J Cardiovasc Imaging, 29: 1575-1584.

86. Mushtaq S, De Araujo Goncalves P, Garcia-Garcia HM, Pontone G, Bartorelli AL, Bertella E, Campos CM, Pepi M, Serruys PW, Andreini D. (2015) Long-term prognostic effect of coronary atherosclerotic burden: validation of the computed tomography-Leaman score. Circ Cardiovasc Imaging, 8: e002332.

87. Douglas PS, Hoffmann U, Patel MR, Mark DB, Al-Khalidi HR, Cavanaugh B, Cole J, Dolor RJ, Fordyce CB, Huang M, Khan MA, Kosinski AS, Krucoff MW,

Malhotra V, Picard MH, Udelson JE, Velazquez EJ, Yow E, Cooper LS, Lee KL, Investigators P. (2015) Outcomes of anatomical versus functional testing for coronary artery disease. N Engl J Med, 372: 1291-1300.

88. Karolyi M, Szilveszter B, Kolossvary M, Takx RA, Celeng C, Bartykowszki A, Jermendy AL, Panajotu A, Karady J, Raaijmakers R, Giepmans W, Merkely B, Maurovich-Horvat P. (2017) Iterative model reconstruction reduces calcified plaque volume in coronary CT angiography. Eur J Radiol, 87: 83-89.

89. Dwivedi G, Liu Y, Tewari S, Inacio J, Pelletier-Galarneau M, Chow BJ. (2016) Incremental Prognostic Value of Quantified Vulnerable Plaque by Cardiac Computed Tomography: A Pilot Study. J Thorac Imaging, 31: 373-379.

90. Versteylen MO, Kietselaer BL, Dagnelie PC, Joosen IA, Dedic A, Raaijmakers RH, Wildberger JE, Nieman K, Crijns HJ, Niessen WJ, Daemen MJ, Hofstra L. (2013) Additive value of semiautomated quantification of coronary artery disease using cardiac computed tomographic angiography to predict future acute coronary syndrome. J Am Coll Cardiol, 61: 2296-2305.

91. Szilveszter B, Celeng C, Maurovich-Horvat P. (2016) Plaque assessment by coronary CT. Int J Cardiovasc Imaging, 32: 161-172.

92. Voros S, Rinehart S, Qian Z, Joshi P, Vazquez G, Fischer C, Belur P, Hulten E, Villines TC. (2011) Coronary atherosclerosis imaging by coronary CT angiography: current status, correlation with intravascular interrogation and meta-analysis. JACC Cardiovasc Imaging, 4: 537-548.

93. Lehman SJ, Schlett CL, Bamberg F, Lee H, Donnelly P, Shturman L, Kriegel MF, Brady TJ, Hoffmann U. (2009) Assessment of coronary plaque progression in coronary computed tomography angiography using a semiquantitative score. JACC Cardiovasc Imaging, 2: 1262-1270.

94. Papadopoulou SL, Neefjes LA, Garcia-Garcia HM, Flu WJ, Rossi A, Dharampal AS, Kitslaar PH, Mollet NR, Veldhof S, Nieman K, Stone GW, Serruys PW, Krestin GP, de Feyter PJ. (2012) Natural history of coronary atherosclerosis by multislice computed tomography. JACC Cardiovasc Imaging, 5: S28-37.

95. Papadopoulou SL, Garcia-Garcia HM, Rossi A, Girasis C, Dharampal AS, Kitslaar PH, Krestin GP, de Feyter PJ. (2013) Reproducibility of computed tomography angiography data analysis using semiautomated plaque quantification software:

implications for the design of longitudinal studies. Int J Cardiovasc Imaging, 29: 1095-1104.

96. de Graaf MA, Broersen A, Kitslaar PH, Roos CJ, Dijkstra J, Lelieveldt BP, Jukema JW, Schalij MJ, Delgado V, Bax JJ, Reiber JH, Scholte AJ. (2013) Automatic quantification and characterization of coronary atherosclerosis with computed tomography coronary angiography: cross-correlation with intravascular ultrasound virtual histology. Int J Cardiovasc Imaging, 29: 1177-1190.

97. Kim YJ, Jin GY, Kim EY, Han YM, Chae JK, Lee SR, Kwon KS. (2013) Quantification of coronary artery plaque using 64-slice dual-source CT: comparison of semi-automatic and automatic computer-aided analysis based on intravascular ultrasonography as the gold standard. Int J Cardiovasc Imaging, 29 Suppl 2: 93-100.

98. Rief M, Kranz A, Hartmann L, Roehle R, Laule M, Dewey M. (2014) Computer-aided CT coronary artery stenosis detection: comparison with human reading and quantitative coronary angiography. Int J Cardiovasc Imaging, 30: 1621-1627.

99. Naoum C, Blanke P, Leipsic J. (2015) Iterative reconstruction in cardiac CT. J Cardiovasc Comput Tomogr, 9: 255-263.

100. Takx RA, Willemink MJ, Nathoe HM, Schilham AM, Budde RP, de Jong PA, Leiner T. (2014) The effect of iterative reconstruction on quantitative computed tomography assessment of coronary plaque composition. Int J Cardiovasc Imaging, 30: 155-163.

101. Fuchs TA, Fiechter M, Gebhard C, Stehli J, Ghadri JR, Kazakauskaite E, Herzog BA, Husmann L, Gaemperli O, Kaufmann PA. (2013) CT coronary angiography: impact of adapted statistical iterative reconstruction (ASIR) on coronary stenosis and plaque composition analysis. Int J Cardiovasc Imaging, 29: 719-724.

102. Puchner SB, Ferencik M, Karolyi M, Do S, Maurovich-Horvat P, Kauczor HU, Hoffmann U, Schlett CL. (2013) The effect of iterative image reconstruction algorithms on the feasibility of automated plaque assessment in coronary CT angiography. Int J Cardiovasc Imaging, 29: 1879-1888.

103. Dey D, Lee CJ, Ohba M, Gutstein A, Slomka PJ, Cheng V, Suzuki Y, Suzuki S, Wolak A, Le Meunier L, Thomson LE, Cohen I, Friedman JD, Germano G, Berman DS. (2008) Image quality and artifacts in coronary CT angiography with dual-source CT: initial clinical experience. J Cardiovasc Comput Tomogr, 2: 105-114.

104. Renker M, Ramachandra A, Schoepf UJ, Raupach R, Apfaltrer P, Rowe GW, Vogt S, Flohr TG, Kerl JM, Bauer RW, Fink C, Henzler T. (2011) Iterative image reconstruction techniques: Applications for cardiac CT. J Cardiovasc Comput Tomogr, 5: 225-230.

105. den Harder AM, Willemink MJ, de Jong PA, Schilham AM, Rajiah P, Takx RA, Leiner T. (2016) New horizons in cardiac CT. Clin Radiol, 71: 758-767.

106. Noel PB, Fingerle AA, Renger B, Munzel D, Rummeny EJ, Dobritz M. (2011) Initial performance characterization of a clinical noise-suppressing reconstruction algorithm for MDCT. AJR Am J Roentgenol, 197: 1404-1409.

107. Hou Y, Liu X, Xv S, Guo W, Guo Q. (2012) Comparisons of image quality and radiation dose between iterative reconstruction and filtered back projection reconstruction algorithms in 256-MDCT coronary angiography. AJR Am J Roentgenol, 199: 588-594.

108. den Harder AM, Willemink MJ, Budde RP, Schilham AM, Leiner T, de Jong PA. (2015) Hybrid and model-based iterative reconstruction techniques for pediatric CT. AJR Am J Roentgenol, 204: 645-653.

109. Lambert L, Ourednicek P, Jahoda J, Lambertova A, Danes J. (2015) Model-based vs hybrid iterative reconstruction technique in ultralow-dose submillisievert CT colonography. Br J Radiol, 88: 20140667.

110. Willemink MJ, Takx RA, de Jong PA, Budde RP, Bleys RL, Das M, Wildberger JE, Prokop M, Buls N, de Mey J, Leiner T, Schilham AM. (2014) Computed tomography radiation dose reduction: effect of different iterative reconstruction algorithms on image quality. J Comput Assist Tomogr, 38: 815-823.

111. Halpern EJ, Gingold EL, White H, Read K. (2014) Evaluation of coronary artery image quality with knowledge-based iterative model reconstruction. Acad Radiol, 21: 805-811.

112. Yuki H, Utsunomiya D, Funama Y, Tokuyasu S, Namimoto T, Hirai T, Itatani R, Katahira K, Oshima S, Yamashita Y. (2014) Value of knowledge-based iterative model reconstruction in low-kV 256-slice coronary CT angiography. J Cardiovasc Comput Tomogr, 8: 115-123.

113. Willemink MJ, de Jong PA, Leiner T, de Heer LM, Nievelstein RA, Budde RP, Schilham AM. (2013) Iterative reconstruction techniques for computed tomography Part 1: technical principles. Eur Radiol, 23: 1623-1631.
114. Willemink MJ, Leiner T, de Jong PA, de Heer LM, Nievelstein RA, Schilham AM, Budde RP. (2013) Iterative reconstruction techniques for computed tomography part 2: initial results in dose reduction and image quality. Eur Radiol, 23: 1632-1642.
115. Oda S, Utsunomiya D, Funama Y, Katahira K, Honda K, Tokuyasu S, Vembar M, Yuki H, Noda K, Oshima S, Yamashita Y. (2014) A knowledge-based iterative model reconstruction algorithm: can super-low-dose cardiac CT be applicable in clinical settings? Acad Radiol, 21: 104-110.
116. Iyama Y, Nakaura T, Iyama A, Kidoh M, Oda S, Tokuyasu S, Yamashita Y. (2017) Usefulness of a Low Tube Voltage: Knowledge-Based Iterative Model Reconstruction Algorithm for Computed Tomography Venography. J Comput Assist Tomogr.
117. Bagyura Z, Kiss L, Edes E, Lux A, Polgar L, Soos P, Szenczi O, Szelid Z, Vadas R, Jozan P, Bagdy G, Merkely B. (2014) [Cardiovascular screening programme in the Central Hungarian region. The Budakalasz Study]. Orv Hetil, 155: 1344-1352.
118. Scheffel H, Stolzmann P, Schlett CL, Engel LC, Major GP, Karolyi M, Do S, Maurovich-Horvat P, Hoffmann U. (2012) Coronary artery plaques: cardiac CT with model-based and adaptive-statistical iterative reconstruction technique. Eur J Radiol, 81: e363-369.
119. Ferencik M, Nomura CH, Maurovich-Horvat P, Hoffmann U, Pena AJ, Cury RC, Abbara S, Nieman K, Fatima U, Achenbach S, Brady TJ. (2006) Quantitative parameters of image quality in 64-slice computed tomography angiography of the coronary arteries. Eur J Radiol, 57: 373-379.
120. Szilveszter B, Elzomor H, Karolyi M, Kolossvary M, Raaijmakers R, Benke K, Celeng C, Bartykowszki A, Bagyura Z, Lux A, Merkely B, Maurovich-Horvat P. (2016) The effect of iterative model reconstruction on coronary artery calcium quantification. Int J Cardiovasc Imaging, 32: 153-160.
121. Kurata A, Dharampal A, Dedic A, de Feyter PJ, Krestin GP, Dijkshoorn ML, Nieman K. (2013) Impact of iterative reconstruction on CT coronary calcium quantification. Eur Radiol, 23: 3246-3252.

122. Gebhard C, Fiechter M, Fuchs TA, Ghadri JR, Herzog BA, Kuhn F, Stehli J, Muller E, Kazakauskaite E, Gaemperli O, Kaufmann PA. (2013) Coronary artery calcium scoring: Influence of adaptive statistical iterative reconstruction using 64-MDCT. Int J Cardiol, 167: 2932-2937.

123. Tatsugami F, Higaki T, Fukumoto W, Kaichi Y, Fujioka C, Kiguchi M, Yamamoto H, Kihara Y, Awai K. (2015) Radiation dose reduction for coronary artery calcium scoring at 320-detector CT with adaptive iterative dose reduction 3D. Int J Cardiovasc Imaging, 31: 1045-1052.

124. Yoo SM, Lee HY, White CS. (2014) Screening coronary CT angiography: possibilities and pitfalls. Int J Cardiovasc Imaging, 30: 1599-1601.

125. Tomizawa N, Nojo T, Inoh S, Nakamura S. (2015) Difference of coronary artery disease severity, extent and plaque characteristics between patients with hypertension, diabetes mellitus or dyslipidemia. Int J Cardiovasc Imaging, 31: 205-212.

126. Tanabe Y, Kido T, Kurata A, Fukuyama N, Yokoi T, Kido T, Uetani T, Vembar M, Dhanantwari A, Tokuyasu S, Yamashita N, Mochizuki T. (2017) Impact of knowledge-based iterative model reconstruction on myocardial late iodine enhancement in computed tomography and comparison with cardiac magnetic resonance. Int J Cardiovasc Imaging.

127. Nadjiri J, Hausleiter J, Jahnichen C, Will A, Hendrich E, Martinoff S, Hadamitzky M. (2016) Incremental prognostic value of quantitative plaque assessment in coronary CT angiography during 5 years of follow up. J Cardiovasc Comput Tomogr, 10: 97-104.

128. Boogers MJ, Broersen A, van Velzen JE, de Graaf FR, El-Naggar HM, Kitslaar PH, Dijkstra J, Delgado V, Boersma E, de Roos A, Schuijf JD, Schalij MJ, Reiber JH, Bax JJ, Jukema JW. (2012) Automated quantification of coronary plaque with computed tomography: comparison with intravascular ultrasound using a dedicated registration algorithm for fusion-based quantification. Eur Heart J, 33: 1007-1016.

129. Diaz-Zamudio M, Fuchs TA, Slomka P, Otaki Y, Arsanjani R, Gransar H, Germano G, Berman DS, Kaufmann PA, Dey D. (2016) Quantitative plaque features from coronary computed tomography angiography to identify regional ischemia by myocardial perfusion imaging. Eur Heart J Cardiovasc Imaging.

10. BIBLIOGRAPHY OF THE CANDIDATE'S PUBLICATIONS

10.1 Publications closely related to the present thesis

1. **Szilveszter B**, Elzomor H, Karolyi M, Kolossvary M, Raaijmakers R, Benke K, Celeng C, Bartykowszki A, Bagyura Z, Lux A, Merkely B, Maurovich-Horvat P. (2016) The effect of iterative model reconstruction on coronary artery calcium quantification. Int J Cardiovasc Imaging, 32: 153-160. IF:1.880

2. Karolyi M*, **Szilveszter B***, Kolossvary M, Takx RA, Celeng C, Bartykowszki A, Jermendy AL, Panajotu A, Karady J, Raaijmakers R, Giepmans W, Merkely B and Maurovich-Horvat P. (2017) Iterative model reconstruction reduces calcified plaque volume in coronary CT angiography. Eur J Radiol. 87:83-89. IF:2.593

3. **Szilveszter B**, Celeng C, Maurovich-Horvat P. (2016) Plaque assessment by coronary CT. Int J Cardiovasc Imaging, 32: 161-172. IF:1.880

10.2 Publications not related to the present thesis

1. Kolossváry M, **Szilveszter B**, Merkely B, Maurovich-Horvat P (2016) Plaque imaging with CT—a comprehensive review on coronary CT angiography based risk assessment. *Cardiovascular Diagnosis and Therapy* 10.21037/cdt.2016.11.06 IF:N/A

2. Meyersohn NM, **Szilveszter B**, Staziaki PV, Scholtz J-E, Takx RAP, Hoffmann U, Ghoshhajra BB (2017) Coronary CT angiography in the emergency department utilizing second and third generation dual source CT. *Journal of Cardiovascular Computed Tomograph* (2017), doi: 10.1016/ j.jcct.2017.03.002. IF: 2,472

3. Janjua SA, Triant VA, Addison D, **Szilveszter B**, Regan S, Staziaki PV, Grinspoon SA, Hoffmann U, Zanni MV and Neilan TG. (2016) HIV Infection and Heart Failure Outcomes in Women. *J Am Coll Cardiol*. 69:107-108. IF: 17.759

4. Farhad H, Staziaki PV, Addison D, Coelho-Filho OR, Shah RV, Mitchell RN, **Szilveszter B**, Abbasi SA, Kwong RY, Scherrer-Crosbie M, Hoffmann U, Jerosch-Herold M and Neilan TG. Characterization of the Changes in Cardiac

Structure and Function in Mice Treated With Anthracyclines Using Serial Cardiac Magnetic Resonance Imaging. *Circ Cardiovasc Imaging*. 2016;9. IF: 5.744

5. Celeng C, Kolossvary M, Kovacs A, Molnar AA, **Szilveszter B**, Horvath T, Karolyi M, Jermendy AL, Tarnoki AD, Tarnoki DL, Karady J, Voros S, Jermendy G, Merkely B and Maurovich-Horvat P. Aortic root dimensions are predominantly determined by genetic factors: a classical twin study. *Eur Radiol*. 2016. IF: 3.640

6. Edes IF, Ruzsa Z, Szabo G, Lux A, Geller L, Molnar L, Nowotta F, Hajas A, **Szilveszter B**, Becker D and Merkely B. Rotational atherectomy of undilatable coronary stents: stentablation, a clinical perspective and recommendation. *EuroIntervention*. 2016;12:e632-5. IF: 3.863

7. Kolossvary M, **Szilveszter B**, Edes IF, Nardai S, Voros V, Hartyanszky I, Merkely B, Voros S and Maurovich-Horvat P. Comparison of Quantity of Coronary Atherosclerotic Plaques Detected by Computed Tomography Versus Angiography. *Am J Cardiol*. 2016;117:1863-7. IF: 3.154

8. Benke K, Agg B, Szabo L, **Szilveszter B**, Odler B, Polos M, Cao C, Maurovich-Horvat P, Radovits T, Merkely B and Szabolcs Z. Bentall procedure: quarter century of clinical experiences of a single surgeon. *J Cardiothorac Surg*. 2016;11:19. IF: 1.036

9. Odler B, Cseh A, Constantin T, Fekete G, Losonczy G, Tamasi L, Benke K, **Szilveszter B** and Muller V. Long time enzyme replacement therapy stabilizes obstructive lung disease and alters peripheral immune cell subsets in Fabry patients. *Clin Respir J*. 2016. IF: 2.147

10. Maurovich-Horvat P, Tarnoki DL, Tarnoki AD, Horvath T, Jermendy AL, Kolossvary M, **Szilveszter B**, Voros V, Kovacs A, Molnar AA, Littvay L, Lamb HJ, Voros S, Jermendy G and Merkely B. Rationale, Design, and Methodological Aspects of the BUDAPEST-GLOBAL Study (Burden of Atherosclerotic Plaques Study in Twins-Genetic Loci and the Burden of Atherosclerotic Lesions). *Clin Cardiol*. 2015;38:699-707. IF: 2.431

11. Csobay-Novak C, Fontanini DM, Szilagyi BR, Szeberin Z, **Szilveszter B**, Maurovich-Horvat P, Huttl K and Sotonyi P. Thoracic aortic strain can affect endograft sizing in young patients. *J Vasc Surg*. 2015;62:1479-84. IF: 3.454

12. Benke K, Agg B, Matyas G, Szokolai V, Harsanyi G, **Szilveszter B**, Odler B, Polos M, Maurovich-Horvat P, Radovits T, Merkely B, Nagy ZB and Szabolcs Z. Gene polymorphisms as risk factors for predicting the cardiovascular manifestations in Marfan syndrome. Role of folic acid metabolism enzyme gene polymorphisms in Marfan syndrome. *Thromb Haemost*. 2015;114:748-56. IF: 5.255

13. Edes IF, Ruzsa Z, Szabo G, Nardai S, Becker D, Benke K, **Szilveszter B** and Merkely B. Clinical predictors of mortality following rotational atherectomy and stent implantation in high-risk patients: A single center experience. *Catheter Cardiovasc Interv*. 2015;86:634-41. IF: 2.181

14. Maurovich-Horvat P, Karolyi M, Horvath T, **Szilveszter B**, Bartykowszki A, Jermendy AL, Panajotu A, Celeng C, Suhai FI, Major GP, Csobay-Novak C, Huttl K and Merkely B. Esmolol is noninferior to metoprolol in achieving a target heart rate of 65 beats/min in patients referred to coronary CT angiography: a randomized controlled clinical trial. *J Cardiovasc Comput Tomogr*. 2015;9:139-45. IF: 2.472

15. Agg B, Benke K, **Szilveszter B**, Polos M, Daroczi L, Odler B, Nagy ZB, Tarr F, Merkely B and Szabolcs Z. Possible extracardiac predictors of aortic dissection in Marfan syndrome. *BMC Cardiovasc Disord*. 2014;14:47. IF: 1.916

16. Benke K, Agg B, **Szilveszter B**, Tarr F, Nagy ZB, Polos M, Daroczi L, Merkely B and Szabolcs Z. The role of transforming growth factor-beta in Marfan syndrome. *Cardiol J*. 2013;20:227-34. IF: 1.470

Articles in Hungarian

1. Benke K , Sayour AA , Ágg B , Radovits T , **Szilveszter B** , Odler B , Németh BT , Pólos M , Oláh A , Mátyás Cs , Ruppert M , Hartyánszky I , Maurovich-Horvat P , Merkely B , Szabolcs Z. (2016) Génpolimorfizmusok, mint

rizikófaktorok a Marfan-szindróma kardiovaszkuláris manifesztációinak előrejelzésében *Cardiologia Hungarica* 46: pp. 76-81. IF:N/A

2. Bartykowszki A, Tóth L, Kerecsen G, Jermendy ÁL, Kolossváry M, Karády J, **Szilveszter B**, Károlyi M, Suhai F, Panajotu A, Kolozsvári R, Balázs Gy, Hüttl K, Thury A, Batthyány I, Kiss RG, Merkely B, Maurovich-Horvat P. (2017) A koronária-CT- angiográfia értelmezése és leletezése. A Magyar Kardiológusok Társasága Kardiovaszkuláris Képalkotó Munkacsoportjának ajánlása. *Cardiologia Hungarica* 47:(1) pp 2-9. IF:N/A
3. Benke K, Ágg B, **Szilveszter B**, Odler B, Nagy Zs, Pólos M, Merkely B, Szabolcs Z. (2014) A Marfan-szindróma molekuláris pathomechanizmusa. *Cardiologia Hungarica* 44(2):115-121. IF:N/A

DOI:10.14753/SE.2017.2079

ACKNOWLEDGEMENTS

The work presented in this thesis would not have been possible without the advice and support of several individuals. I would like to extend my sincere gratitude and appreciation to all those who made this PhD thesis possible.

First and foremost, I would like to thank to my mentor and supervisor Pál Maurovich-Horvat for his guidance and continued support during my PhD years. I am truly fortunate to learn from such an inspiring teacher and outstanding researcher. I will remain forever grateful.

I would like to express my sincere gratitude to Prof. Béla Merkely for giving me the opportunity to carry out my research projects and who also provided the intellectual, financial, professional background required for my research career.

I am also grateful to my friends, Kálmán Benke, Júlia Karády and Márton Kolossváry for their helpful suggestions, advices and for all the encouragement and support they gave to me during my PhD years. You have inspired and motivated me during difficult times.

I would like to thank Mihály Károlyi for his contribution and collaborative work. Without his support and constant feedback this PhD would not have been achievable.

Also, I would like to express my thanks to all my former and current colleagues at the Heart and Vascular Center for their support and contribution to my research.

It has been a privilege to work with Prof. Udo Hoffmann and his research team in Boston. Thank you for allowing me to participate in his Program and also for teaching me the importance and value of precision, concept, design and hard work in research. Thank you for this amazing experience and an exceptional opportunity to work with the members of the Cardiac MR PET CT Program and the MGH faculty. I would like to thank Drs. Brian Ghoshhajra, Michael Lu and Tomas Neilan for their help and support that paved the way

DOI:10.14753/SE.2017.2079

for our successful collaboration. I am looking forward for further collaborations with such an inspiring and excellent team.

A very special word of thanks goes to Szabina for her unconditional love, encouragement and unending patience.

Finally, I would like to thank to my Parents and my Brother for helping in whatever way they could during this challenging period and provided a carefree and loving environment for me.